UNIVERSIDAD DE INVESTIGACIÓN DE TECNOLOGÍA EXPERIMENTAL YACHAY

Escuela de Ciencias Físicas y Nanotecnología

PHOTOINDUCED QUANTUM TRANSPORT

Trabajo de integración curricular presentado como requisito para la obtención del título de Física

Autor: Jeyson Patricio Alomoto Catota

Tutor: Ph.D. Duncan J. Mowbray

Co-tutor: Ph.D. Vito Despoja

Urcuquí, agosto 2024

Autoría

Yo, **Alomoto Catota Jeyson Patricio**, con cédula de identidad 0504008731, declaro que las ideas, juicios, valoraciones, interpretaciones, consultas bibliográficas, definiciones y conceptualizaciones expuestas en el presente trabajo; así cómo, los procedimientos y herramientas utilizadas en la investigación, son de absoluta responsabilidad de el/la autora (a) del trabajo de integración curricular. Así mismo, me acojo a los reglamentos internos de la Universidad de Investigación de Tecnología Experimental Yachay.

Urcuquí, agosto 2024.

<div style="text-align:center">

―――――――――――――――――

Jeyson Patricio Alomoto Catota

CI:0504008731

</div>

Autorización de publicación

Yo, **Alomoto Catota Jeyson Patricio**, con cédula de identidad 0504008731, cedo a la Universidad de Investigación de Tecnología Experimental Yachay, los derechos de publicación de la presente obra, sin que deba haber un reconocimiento económico por este concepto. Declaro además que el texto del presente trabajo de titulación no podrá ser cedido a ninguna empresa editorial para su publicación u otros fines, sin contar previamente con la autorización escrita de la Universidad. Asimismo, autorizo a la Universidad que realice la digitalización y publicación de este trabajo de integración curricular en el repositorio virtual, de conformidad a lo dispuesto en el Art. 144 de la Ley Orgánica de Educación Superior

Urcuquí, agosto 2024.

———————————————————

Jeyson Patricio Alomoto Catota

CI:0504008731

Acknowledgements

Resumen

Dispositivos solares más baratos con mayores eficiencias solo pueden construirse realizando esfuerzos continuos para desarrollar nuevos materiales que puedan superar la eficiencia del silicio (Si) a un costo razonable. El transporte cuántico fotoinducido sigue siendo un campo abierto para el desarrollo de ciencia de alto impacto y con gran importancia economica a nivel global. Los modelos computacionales actuales pueden ser útiles para un gran conjunto de aplicaciones relacionados a la física y se han vuelto cruciales para acelerar cualquier proceso de investigación. El trabajo actual propone un modelo para calcular la eficiencia cuántica externa (EQE) teóricamente, proporcionando un método simple para comparar la eficiencia de diferentes materiales semiconductores. La EQE se define como la fracción de electrones transmitidos respecto a los fotones incidentes en la celda solar, $\eta_{EQE} = \frac{N_e}{N_\omega}$, y puede utilizarse para medir la capacidad de un material para producir portadores de carga cuando es irradiado con luz.

El modelo se basa en el formalismo de la función de Green fuera del equilibrio (NEGF) para describir el transporte cuántico. El modelo incluye un operador $\hat{\mathcal{A}}(\mathbf{r}, t) = \frac{e}{2mc}\hat{\mathbf{A}}.\hat{\mathbf{p}}$, definido como la interacción dependiente del tiempo que actúa como un acoplamiento entre los estados ocupados y desocupados a través del campo electromagnético externo $\langle \varphi_\mu | \hat{\mathcal{A}}(\mathbf{r}, t) | \varphi_v \rangle$.

Este modelo se aplicó sobre un arreglo de dos y cuatro moléculas de [6,6] fenil-C61-ácido butírico metil éster (PCBM) utilizando condiciones de contorno periódicas con luz polarizada en cada dirección. Nuestros cálculos de teoría del funcional de la densidades (DFT) emplean la combinación lineal de orbitales atómicos (LCAO) para representar las funciones de onda de Kohn-Sham, la aproximación de gradiente generalizado (GGA) de Perdew, Burke y Ernzerhof (PBE) para el funcional de intercambio y correlación (xc), las correcciones semiempíricas D3 de Grimme para describir las interacciones de van der Waals y la corrección de la discontinuidad derivativa para ajustar el gap energético de la DFT.

Nuestros resultados sugieren una EQE significativa para fotones con energías entre 2.8 y 3.8 eV, lo que corresponde al rango del ultravioleta cercano (UV). Además, en el rango de energía de 0 a 4 eV, la transmisión va del 1 al 5% en las zonas donde los estados ocupados y desocupados muestran una fuerte superposición. Para investigaciones futuras, el modelo puede utilizarse en paralelo con inteligencia artificial para analizar grandes conjuntos de bases de datos buscando aquellos materiales con alta EQE para su diseño *in silico*.

Palabras clave: Eficiencia, modelo computacional, funciones de Green, transmisión.

Abstract

Cheaper solar devices with higher efficiencies can only be constructed by making continuous efforts to develop novel materials that can surpass the efficiency of silicon (Si) at a reasonable cost. Photoinduced quantum transport is still an open field for developing high-impact science of great importance globally. Current computational models can be helpful for a large set of physical applications and have become crucial for accelerating any investigation process. The current work proposes a model to calculate external quantum efficiency (EQE) theoretically, providing a simple method for comparing the efficiency of different semiconductor materials. EQE is defined as the fraction of transmitted electrons to incident photons in the solar cell, $\eta_{EQE} = \frac{N_e}{N_\omega}$, and can be used to measure the capability of a material to produce charge carriers when it is irradiated with light. The model is constructed using the non-equilibrium Green's function (NEGF) formalism to describe the quantum transport. The model includes an operator $\hat{\mathcal{A}}(\mathbf{r}, t) = \frac{e}{2mc}\hat{\mathbf{A}}.\hat{\mathbf{p}}$ defined as the time-dependent interaction which acts as a coupling between the occupied and unoccupied states via the external electromagnetic field as $\langle \varphi_\mu | \hat{\mathcal{A}}(\mathbf{r}, t) | \varphi_\nu \rangle$. This model was applied over an arrangement of two and four [6,6] phenyl-C61-butyric acid methyl ester (PCBM) molecules using periodic boundary conditions with light polarized in each direction. Our density functional theory (DFT) calculations employ a linear combination of atomic orbitals (LCAO) to represent the Kohn-Sham wavefunctions, the generalized gradient approximation (GGA) implementation of Perdew, Burke, and Ernzerhof (PBE) for the exchange and correlation (xc) functional, Grimme's semi-empirical D3 corrections to describe van der Waals interactions and the derivative discontinuity correction to correct the DFT energy gap. Our results suggest an important EQE for photons with energies between 2.8 and 3.8 eV, which corresponds to the near ultraviolet (UV) range. Moreover, in the energy range from 0 to 4 eV, the transmission goes from 1 to 5% in the places where the occupied and unoccupied states show strong overlapping. For further research, the model can be used in parallel with artificial intelligence to analyze large sets of databases looking for those materials with high EQE for their design in silico.

Keywords: efficiency, computational model, Green's Functions, transmission.

Contents

List of Figures

List of Papers

[1] Duncan J. Mowbray, Jeyson P. Alomoto-Catota, Daniel E. Gonzalez-Tamayo, and Vito Despoja, "Photoinduced Quantum Transport" (in progress 2024).

Chapter 1

Introduction

The Ecuadorian energy industry still needs decades to reach competitiveness in the international market. The majority of Ecuadorian electricity production comes from hydroelectric sources. According to the Ministry of Energy and Mines, Ecuadorian energy is obtained as 92% from hydroelectric, 7% from thermal, and only 1% comes from photovoltaics, wind, biomass, biogas, geothermal, etc[1]. It is critical to increase investments in new technologies to solve future energetic production problems and be less dependent on Ecuadorian hydro-electrics. The development of novel photovoltaic cells can be the solution to diversifying electricity sources since Ecuador has 12 hours of sunlight year-round.

Photovoltaic cells are electronic devices that transform light into electricity by the photoelectric effect. When the photons hit the solar cell, electrons are excited from the valence band to the conduction band producing electron-hole pairs. Typically, solar cells are made of semiconductor materials in a p-n junction. Usually, these junctions are doped by creating a majority of electrons in the n-type, and a greater number of holes in the p-type. The most commonly known solar cell is made using silicon, but there exist many other possible solar cell types such as organic solar cells, dye solar cells, perovskite solar cells, quantum dot solar cells, etc. In all cases, an array of solar cells turns light into direct current (DC) electricity. Although there are many options to construct solar cells, only a few materials can transform solar energy into current and voltage with high efficiency at a low cost[2].

Emerging photovoltaic technologies are still in the development phase and are yet to be introduced in the market. Many of the appearing organic materials still have low efficiencies for

commercial purposes. Nevertheless, the research in this technology wants to achieve low-cost production and high efficiency for the near future[3].

Historically, the high costs of producing photovoltaic cells are due to the semiconductor industry. In 1970 a solar module cost around $96 per watt. Nevertheless, with the advance of technology and increased investment in research, the prices dropped to $0.3 per watt in 2018 and $0.2 in 2020[4]. This means that nowadays solar cells have become an interesting option to produce clean energy worldwide. North America, Europe, Asia, and many other countries are leading solar energy production and making huge investments in research to improve the current technology. The study of electronics, semiconductors, solar cells, and other topics related to physics is crucial for the development of novel materials. Soon, the costs of production of such materials will be reduced as a result of the semiconductor industry capacity.

One common approach for comparing and ranking solar cells is the external quantum efficiency (EQE). This is a measurement of the capability of a material to produce current when it is irradiated with light. The EQE is defined as the fraction of the transmitted electrons to incident photons on the solar cell[5]. In this thesis, the formalism for calculating EQE will be to use Non-Equilibrium Green's Functions (NEGF). Since NEGF is a well-established formalism to model quantum transport in different systems[6], we will use it for the EQE calculation in [6,6] phenyl-C61-butyric acid methyl ester (PCBM). In this context, having a model to calculate EQE from ab-initio in many materials would be very advantageous. This is because the calculations are made on the same footing, making it possible to compare the EQE for a large set of candidate materials and choose the best ones for experimental testing.

This thesis primarily proposes a theoretical and computational model to calculate EQE. This model is applied to an organic photovoltaic material (OPV) PCBM. Nevertheless, it can be used for a large range of materials perhaps even using artificial intelligence to search for materials that have a high EQE.

In the case of PCBM, it is an acceptor material of n-type that can be blended with polymers of p-type to create solar cells[7]. Normally, PCBM is more used than fullerenes as an acceptor material because it is easier to create donor-acceptor mixes due to its solubility in chlorobenzene. Nonetheless, the costs of production of PCBM are still an obstacle to its mass production for photovoltaic applications. The experimental efficiency of PCBM solar cells is above 4%[8]. Since the experimental EQE of PCBM is well known, the simulation results can be easily compared.

Our computational approach to obtain the EQE is based on density-functional theory (DFT) calculations employing the projector augmented wave (PAW) method code GPAW. The PAW method is a computational technique to recover the all-electron density of atoms and molecules. It is based on the statement that wave functions oscillate swiftly near the nucleus, whereas close to the bonding region they are rather smooth[9]. Additionally, we are using the atomic simulation environment (ASE), which is a software package designed to facilitate the configuration, control, and examination of atomistic simulations. It facilitates computations related to energy, forces, stresses, and various other parameters by establishing connections to numerous external electronic structure codes or force fields. ASE offers modules that enable the execution of common simulation procedures, including structural optimization and molecular dynamics, among others[10].

1.1 Problem Statement

The area of photovoltaic cells is quickly evolving, but can still benefit from improvements. Although there exist experimental ways to contain material's EQE, we also needed a computational ab initio method to represent photoinduced quantum transport simulations of semiconducting materials to optimize their design in silico. The NEGF formalism offers a procedure to describe quantum transport. In this thesis we will present a model for calculating EQE with the inclusion of a vector potential working as a coupling between occupied and unoccupied states via the vector potential of the external electromagnetic field **A**. This method will provide a theoretical EQE for photovoltaic devices, based on which it will be possible to design materials with higher EQEs in silicon.

1.2 General and Specific Objectives

Currently, accurate and efficient ab initio methods for calculating a material's EQE are still lacking. The main objective of this thesis is to contribute to solving this problem by constructing a method to calculate EQE computationally. The treatment of this method allows us to obtain computational efficiency in quantum transport for photovoltaic devices. It can be used to rank the efficiency of different photovoltaic materials, i.e., design higher EQE materials in silico, for

experimental physicists. The contribution to the photovoltaic devices of this thesis includes the EQE analysis of an arrangement of 2 PCBM and 4 PCBM.

Also, this thesis aims to prove computationally that this model can be applied to a large set of semiconducting materials, encouraging research in materials like silicon, germanium, nanoribbons, carbon nanotubes, etc. This work wants to be the first collaboration to construct a tool capable of finding better semiconducting materials for constructing photovoltaics with higher efficiencies in the near future.

1.3   Overview

This thesis has five chapters and an appendix. Chapter 1 is the introduction. Here we began by discussing the lack of photovoltaic industry capacity in Ecuador. Additionally, it briefly explained what a photovoltaic cell is, its composition, history, and how it works. Also, is explained shortly what is EQE and how the NEGF describes quantum transport. Furthermore, is explained the PAW and ASE which are the computational resources to develop the model. Lastly, is explained how the development of a computational model to calculate EQE is still an open problem.

Chapter 2 describes the relevant theoretical background for EQE calculations. The topics treated are many body problems, periodic systems, Bohr Oppenheimer approximations, the Hohenberg Kohn theorem, Kohn Sham self-consistent field approach, exchange-correlation functional, derivative discontinuity, Band gap, GLL, GLLBsc, LCAO, Green's functions, Nonequilibrium Green's functions, projector augmented method and the basic theory of materials about PCBM.

Chapter 3 explains the methodology and the computational details for the model employed. Specifically, it explained how the PCBM was treated to obtain results, among all the computational resources and physics theory of the model. Chapter 4, here we provide our results and discussion. Here we analyze the density of states of the occupied and unoccupied energy levels, the absorption and transmission probabilities, the excitation energies, and the EQE of the arrangement of the 2 PCBMs.

Finally, Chapter 5 provides conclusions, summarizes the principal results, and provides an outlook for future research.

Chapter 2

Theoretical Background

2.1 Density Functional Theory

2.1.1 Many body problem

Quantum mechanics is the most powerful tool to describe physics in the quantum regime. Schrodinger equations describe the physics behind this world with high probabilistic accuracy. In this case, we are treating a system of many electrons, protons, and their interactions, therefore it is necessary to introduce the "many-body wave function" which is useful to determine observables for physical systems. The wavefunction, Ψ depends on the positions of each electron and proton in the system. Then, in a system there are $\mathbf{r}_1, \mathbf{r}_2, ...\mathbf{r}_N$ for N electrons, and M nuclei with $\mathbf{R}_1, \mathbf{R}_2...\mathbf{R}_M$ obtaining:

$$\Psi = \Psi(\mathbf{r}_1, \mathbf{r}_2, ..., \mathbf{r}_N; \mathbf{R}_1, \mathbf{R}_2, ..., \mathbf{R}_M) \tag{2.1}$$

Now reconstructing the Schrodinger equation with the kinetic and potential energy contributions for all the interactions including one particle case and all the possible interactions of electrons and nuclei[11] $e - e, e - n, n - n$:

$$\mathcal{H}\Psi = E_{tot}\Psi \tag{2.2}$$

where the Hamiltonian has the form

$$\mathcal{H} = -\sum_i \frac{\hbar^2}{2m_e}\nabla_i^2 - \sum_I \frac{\hbar^2}{2M_I}\nabla_I^2 + \frac{1}{2}\sum_{i \neq j} \frac{e^2}{4\pi\epsilon_0} \frac{1}{|\mathbf{r}_i - \mathbf{r}_j|} + \frac{1}{2}\sum_{I \neq J} \frac{e^2}{4\pi\epsilon_0} \frac{Z_I Z_J}{|\mathbf{R}_I - \mathbf{R}_J|} - \sum_I \frac{e^2}{4\pi\epsilon_0} \frac{Z_I}{|\mathbf{r}_i - \mathbf{R}_I|} \tag{2.3}$$

where m_e is the mass of the electron and M_I is the mass of the Ith nucleus, Z_I and Z_J are the atomic numbers of the Ith and Jth nuclei, respectively, and ∇_i^2 and ∇_I^2 are the Laplace operators for the electronic and nuclear coordinates, respectively[12].

2.1.2   Periodic Systems

When density functional theory is used to describe the electronic structure of periodic systems, the application of Bloch's theorem to the Kohn-Sham wavefunctions facilitates the computations. This is because, instead of needing a very large number of electrons, it is only necessary to consider the number of electrons within a single periodic unit cell[13]. From the basic knowledge of solid state physics is well known that a periodic arrangement of atoms in a crystal is described by the unit cell and the lattice points which are invariant under translations. Lattice points are described by:

$$\mathbf{R} = n_1\mathbf{a}_1 + n_2\mathbf{a}_2 + n_2\mathbf{a}_2 \tag{2.4}$$

Where n_1, n_2, n_3 are integers and $\mathbf{a}_1, \mathbf{a}_2, \mathbf{a}_3$ are the lattice vectors spanning in the three-dimensional unit cell with volume Ω.

$$\Omega = |\mathbf{a}_1.(\mathbf{a}_2 \times \mathbf{a}_3)| \tag{2.5}$$

Then three-dimensional crystal remains invariant under translations $\mathbf{R}$, and this crystal symmetry can be exploited using Bloch's Theorem.

Bloch's theorem : From the translational invariance of the crystal, it follows that the electronic wave functions can change only up to a phase factor under translation. This theorem is especially important for systems with a periodic potential because it states that the solutions of the Schrodinger equation must be of a special form:

$$\psi_\mathbf{k}(\mathbf{r}) = u_\mathbf{k} \exp(i\mathbf{k} \cdot \mathbf{r}) \tag{2.6}$$

where $u_\mathbf{k}(\mathbf{r})$ has the periodicity of the crystal lattice, i.e., $u_\mathbf{k}(\mathbf{r}) = u_\mathbf{k}(\mathbf{r} + \mathbf{R})$, with $\mathbf{R}$ as the translation vector of the lattice, $\exp(i\mathbf{k} \cdot \mathbf{r})$ is the plane wave and $\mathbf{k}$ is the crystal momentum. If a translation acts on a wave function, its crystal momentum does not change[14]. Now for every set of $\mathbf{R}$ of lattice points is constructed a reciprocal lattice described by its reciprocal lattice vectors $\mathbf{b}_1, \mathbf{b}_2, \mathbf{b}_3$, defined by

$$\mathbf{a}_i \cdot \mathbf{b}_j = 2\pi\delta_{ij} \tag{2.7}$$

and $\mathbf{b}_i$ can be obtained as

$$\mathbf{b}_i = 2\pi \frac{\mathbf{a}_{i+1} \times \mathbf{a}_{i+2}}{\Omega} \tag{2.8}$$

2.1.3 Born-Oppenheimer Approximation

The Born-Oppenheimer approximation works with the assumption that the nuclei can be treated as classical particles. This can be done because the mass of the nucleus is much larger than the mass of the electrons. Then is understood that the positions of the nuclei are essentially fixed while the positions of the electrons are dynamic. It consists of writing the total wave function using the technique of separation of variables. Then it is possible to write Ψ_{tot} as the product of the electronic wave function and the nuclear wave function

$$\Psi_{tot} = \psi_e^{\mathbf{R}_1,...,\mathbf{R}_M}(\mathbf{r}_1, ..., \mathbf{r}_N)\psi_n(\mathbf{R}_1, ..., \mathbf{R}_M) \tag{2.9}$$

where ψ_e and ψ_n represent the electronic and nuclear wavefunctions respectively. The electronic wavefunction ψ_e is the solution to the electronic Schrödinger equation[15]:

$$H_e\psi_e^{\mathbf{R}_1,...,\mathbf{R}_M}(\mathbf{r}_1, ..., \mathbf{r}_N) = E_e\psi_e^{\mathbf{R}_1,...,\mathbf{R}_M}(\mathbf{r}_1, ..., \mathbf{r}_N) \tag{2.10}$$

where the electronic wave function depends directly on the electronic coordinates but only parametrically on the nuclear coordinates. Using E_e as the eigen-energies and H_e as the electronic Hamiltonian[16]. Therefore this system can be solved more efficiently.

2.1.4 Hohenberg-Kohn Theorem

In 1964 Hohenberg and Kohn demonstrated that there exists a direct relation between the electronic density and the external potential $v_{ext}(\mathbf{r})$ for the ground state energy. They concluded that the energy of the ground electronic state is a unique function of the electron density[17]. In their paper, they state that a collection of electrons moving due to the influence of an external potential V_{ext} has the following Hamiltonian.

$$\mathcal{H} = T + U + V_{ext} \tag{2.11}$$

$$T = \frac{1}{2} \int \nabla\psi^*(\mathbf{r})\nabla\psi(\mathbf{r})d\mathbf{r} \tag{2.12}$$

$$U = \frac{1}{2} \int \frac{1}{|\mathbf{r} - \mathbf{r}'|} \psi^*(\mathbf{r})\psi^*(\mathbf{r}')\psi(\mathbf{r}')\psi(\mathbf{r})d\mathbf{r}d\mathbf{r}' \tag{2.13}$$

$$V_{ext} = \int v(\mathbf{r})\psi^*(\mathbf{r})\psi(\mathbf{r})d\mathbf{r} \tag{2.14}$$

Then define the electronic density in the ground state ψ by:

$$n(\mathbf{r}) = \langle \psi|\hat{n}|\psi \rangle \tag{2.15}$$

Since ψ is a functional of n($\mathbf{r}$) we define:

$$F[n(\mathbf{r})] = \langle \psi|(T + U)|\psi \rangle \tag{2.16}$$

using $F[n]$ as a universal functional for any potential and number of particles. It contains the kinetic energy T and the electron-electron interaction U. Therefore, for a given potential $v_{ext}(\mathbf{r})$, the energy potential is given by:

$$E[n] = \int v_{ext}(\mathbf{r})n(\mathbf{r})d\mathbf{r} + F[n] \tag{2.17}$$

The total energy $E[n]$ is the ground state energy and only depends on the electronic density.[18]

2.1.5   Kohn-Sham Self-consistent Field Approach

To approximate the Schrödinder equation, many methods to calculate the solid-state properties have been developed in recent decades. The DFT theory calculations using the Kohn-Sham approach determine a density by using "self-consistency". The concept of self-consistency is born with the so-called mean-field approximation, also called the Hartree potential. This "mean-field potential" is generated by the charge distribution of the system and replaces the two-body Coulomb interaction between charged particles[19]. The Hartree potential or mean-field reaches self-consistency when the initial field and the final field are the same[20].

The first objective is to compute the particle density $\rho(x)$ for some atoms and positions. The particle density is defined by single-particle orbitals $\phi(x)$.

$$\rho(x) = \sum_{i=1}^{N} |\phi_i(x)|^2 \tag{2.18}$$

Next, a set of N particles in the system are influenced by an external potential v_{ext} which is defined by species, positions of the atoms, approximation level, etc. Also, the ground state energy E is possible to calculate.

Now it is possible to introduce the *Kohn-Sham equations*,

$$H_{KS}[\rho] = -\frac{1}{2}\nabla^2 + v_{eff}(\mathbf{r};\rho) \tag{2.19}$$

$$v_{eff} = v_{ext}(\mathbf{r}) + v_h[\rho] + v_{xc}[\rho] \tag{2.20}$$

$$v_h[\rho](x) = \int \frac{\rho(x')}{|x - x'|} \tag{2.21}$$

$$v_{xc}[\rho] = \frac{\delta\epsilon_{xc}}{\delta\rho} \tag{2.22}$$

and the Kohn Sham Hamiltonian introduced in the Schrödinger equation is

$$H_{KS}[\rho]\phi_i(x) = \epsilon_i\phi_i(x) \tag{2.23}$$

Now, to construct the Kohn Sham Hamiltonian it is needed an initial density ρ^{in} as the input to compute the mean field and exchange-correlation potentials. Then, an output density ρ^{out} is calculated from the eigenfunctions of the Kohn-Sham Hamiltonian

$$H_{KS}[\rho^{in}]\phi_i(x) = \epsilon_i\phi_i(x) \tag{2.24}$$

and

$$\rho^{out}(x) = \sum_{i=1}^{N} |\phi_i(x)|^2 \tag{2.25}$$

which is an iterative process that uses an initial estimate of density as input and iterates it across a self-consistent solution of the Kohn-Sham equations.

Initially, as depicted in Figure 2.1 the input density is not equal to the output density for a given potential and exchange-correlation functional. Self-consistency is reached after some iterations $\rho^{in} = \rho^{out}$ and hence the Eqs. 2.15 and 2.16 can be solved[20].

Initial guess density ρ_0^{in}

$$\rho^{in} = \rho_0^{in}$$

Solving:

$$H_{KS}[\rho^{in}]\phi_i(x) = \epsilon_i\phi_i(x)$$

$$\rho^{in} = \rho^{out}$$

Generate a:

$$\rho^{out}(x) = \sum_{i=1}^{N}|\phi_i(x)|^2$$

Is $\rho^{in}(x) \approx \rho^{out}(x)$?

Exit $\rho^{in} = \rho^{out}$
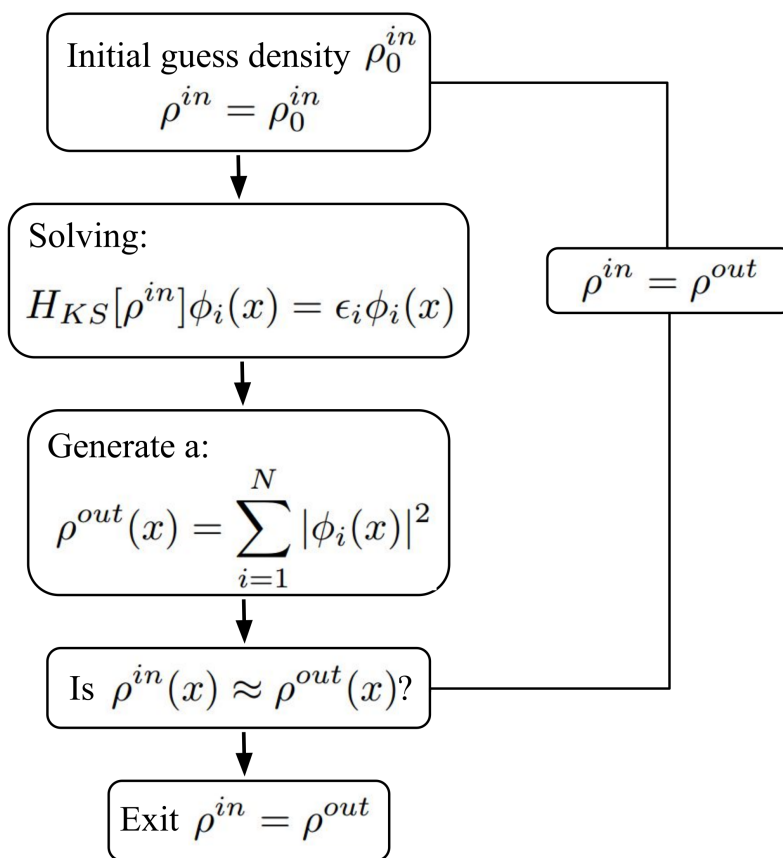
Figure 2.1: Self-consistent Kohn-Sham scheme. Adapted from ref[21]

2.1.6 Exchange-correlation functionals

Ideally, an approximate density functional $E_{xc}[n \uparrow, n \downarrow]$ should have all of the following features: (1) a non-empirical derivation, since the principles of quantum mechanics are well-known and sufficient; (2) universality, since in principle one functional should work for diverse systems (atoms, molecules, solids) with different bonding characters (covalent, ionic, metallic, hydrogen, and van der Waals); (3) simplicity, since this is our only hope for intuitive understanding and our best hope for practical calculation; and (4) accuracy enough to be useful in calculations for real systems. The energy functional is given by[22]

$$E_v[\rho] = \sum_i \epsilon_i - \int \int \frac{\rho(\mathbf{r})\rho(\mathbf{r'})}{|\mathbf{r} - \mathbf{r'}|} d\mathbf{r} d\mathbf{r'} + E_{xc}[\rho] - \int d\mathbf{r}\rho(\mathbf{r}) \frac{\delta E_{xc}}{\delta\rho(\mathbf{r})} \qquad (2.26)$$

and the exchange-correlation potential is

$$v_{xc}(\mathbf{r}) = \frac{\delta E_{xc}[\rho]}{\delta\rho(\mathbf{r})} \qquad (2.27)$$

Nevertheless, despite the Honenberg-Kohn-Sham being an exact theory, the problem lies in the fact that the exact expressions for E_{xc} and v_{xc} are not known. Therefore the exchange-correlation energy and potential needs to be approximated[23]. There exists a lot of proposed approximations for the exchange and correlation functionals, they can be classified into families: the local density approximation (LDA), generalized gradient approximation (GGA), meta-GGA, and hybrid.

Local density approximation

The first technique to approximate those quantities is the Local Density Approximation or LDA, in which the exchange-correlation energy E_{xc} only depends on local density[24]. It consists of replacing the exchange-correlation energy by

$$E_{xc}[\rho] = \int d\mathbf{r}\rho(\mathbf{r})\epsilon_{xc}[\rho(\mathbf{r})] \qquad (2.28)$$

in which the $\epsilon_{xc}[\rho(\mathbf{r})]$ is the exchange-correlation energy density of a homogeneous electron gas.

Then in LDA the exact density around an electron at $\mathbf{r}$ is replaced by the density of the homogeneous electron gas $\rho(\mathbf{r})$ as

$$\rho(\mathbf{r'})[f(\mathbf{r},\mathbf{r'}) - 1] \rightarrow \rho(\mathbf{r'})[f(\mathbf{r} - \mathbf{r'}); \rho(\mathbf{r'}) - 1] \tag{2.29}$$

with f as the pair correlation function. LDA is expected to work well when density varies slowly in space as

$$k_f^{-1} \left| \frac{\delta \rho}{\rho} \right| \ll 1 \tag{2.30}$$

with

$$k_f = (3\pi^2 \rho)^{\frac{1}{3}} \tag{2.31}$$

now introducing the relative coordinate $R = r - r'$ one obtains:

$$E_{xc}[\rho] = \frac{e^2}{2} \int d\mathbf{r} \rho(\mathbf{r}) \int R^{-1} \rho_{xc}(\mathbf{r}, \mathbf{R}) d\mathbf{R} \tag{2.32}$$

with

$$\rho_{xc}(\mathbf{r}, \mathbf{R}) = \int \rho(\mathbf{r} + \mathbf{R})[f(\mathbf{r}, \mathbf{r} + \mathbf{R}) - 1] d\Omega_{\mathbf{R}} \tag{2.33}$$

finally considering the integral

$$\int \frac{\rho_{xc}(\mathbf{r}, \mathbf{R})}{\mathbf{R}} = \langle \frac{1}{\mathbf{R}} \rangle \tag{2.34}$$

if this inverse extension is approximated correctly, the LDA approximation is complete[25].

Generalized gradient approximation

The local spin density approximation (LSD) for the exchange-correlation energy, was proposed in the original work of Kohn and Sham and has proved to be remarkably accurate, useful, and hard to improve upon. The generalized gradient approximation (GGA), is a kind of simple extension of LSD[26].

In 1996, Perdew, Burke, and Ernzerhof (PBE) showed how to construct GGA in a simple form and derivation starting by writing the correlation energy in the form:

$$E_c^{GGA}[n \uparrow, n \downarrow] = \int d^3 rn[e_c(r_s, \zeta) + H(r_s, \zeta, t)] \tag{2.35}$$

Where $n \uparrow$, $n \downarrow$, are the spin densities. Also e_c is the correlation energy per electron of the unit gas, r_s is the Seitz radius defined as the radius of a sphere which on average contains one electron

and ζ represents the relative spin polarization given by:

$$\zeta = \frac{n\uparrow - n\downarrow}{n\uparrow + n\downarrow} \qquad (2.36)$$

t is the reduced density gradient

$$t = \frac{|\delta n|}{2\phi(\zeta)k_s n} \qquad (2.37)$$

with $1/k_s$ as the screening length. Additionally, H can be written as

$$H = c_0 \phi^3 ln[1 + \frac{\beta_{MB}}{c_0}t^2[\frac{1 + At^2}{1 + At^2 + A^2 t^4}]] \qquad (2.38)$$

With A as

$$A = \frac{\beta MB}{c_0}\frac{1}{\exp[-e_c(r_s, \zeta)/c_0\phi^3] - 1} \qquad (2.39)$$

On the other hand, the exchange energy is given by:

$$E_x^{GGA}[n] = A_x \int d^3 r n^{\frac{4}{3}} F_x(s) \qquad (2.40)$$

with $F_x(s)$ as

$$F_x(s) = 1 + k - \frac{k}{(1 + \frac{\mu s^2}{k})} \qquad (2.41)$$

where k is a constant less or equal to 0.804. And

$$A_x = -\frac{3}{4\pi}(3\pi^2)^{\frac{1}{3}} \qquad (2.42)$$

There have been many interesting tests and applications of GGA to a wide range of atoms, molecules, and solids. In most systems, the exact exchange-correlation hole is reasonably localized around its electron, as it is in LSD or GGA – and that fact is one of the reasons why LSD and GGA work as well as they do[23].

2.1.7   Derivative discontinuity

Derivative discontinuities can be understood as the change of the exchange-correlation energies concerning an integer number of electrons. The electronic energy of quantum systems shows derivative discontinuities as a consequence of the integer nature of electrons. The derivative

discontinuity of the total energy is a function of the total number of electrons[27]. Looking at eq. 2.22 can be seen that the exchange-correlation potential v_{xc} is given by the functional derivative of the exchange-correlation energy. However, E_{xc} is unknown and then has to be approximated using functionals. The main idea is that the functionals give an approximation for the exchange-correlation energy E_{xc}, potential v_{xc} and therefore gives rise to an approximate density $\rho(\mathbf{r})$. Perder, Parr, Levy, and Balduz demonstrated that the energy for a fractional electron number system is given by a straight line connecting integer electron numbers

$$E(N + \delta) = (1 - \delta)E(N) + \delta E(N + 1) \tag{2.43}$$

$$\rho_{n+\delta}(\mathbf{r}) = (1 - \delta)\rho_N(\mathbf{r}) + \delta\rho_{N+1}(\mathbf{r}) \tag{2.44}$$

This implies that the energy and density can show derivative discontinuities at the integers. This phenomenon occurs when the bond orbitals are energetically different. It can be seen in closed shell molecules where the density difference of the last electron added ($\rho_N - \rho_{N-1}$) is spatially different from where the next electron is added ($\rho_{N+1} - \rho_N$). The exact Kohn-Sham potential undergoes a jump using a constant when it finds an integer. This constant, C, is the derivative discontinuity as $\epsilon \to 0$

$$v_{xc}^{N-\epsilon}(\mathbf{r}) = v_{xc}^N(\mathbf{r}) \tag{2.45}$$

$$v_{xc}^{N+\epsilon}(\mathbf{r}) = v_{xc}^N(r) + C \tag{2.46}$$

For example, if the potential of LDA functional is shifted by a constant, the eq 2.24 will give rise to identical orbitals and density, however, eigenvalues are shifted by C. Then if those orbitals and density are included in eq2.26 will be obtained an identical energy. Therefore, there is a discontinuous change only in eigenvalues, not in the total energy[28].

2.1.8 Band Gap

A basic property of a solid is its band gap G, which is positive for semiconductors and insulators and disappears for metals. The band gap G can be seen as the lowest single electron excitation energy of a solid, representing the conductivity, optical, and thermal properties. The G is an excitation energy and a difference of ground state energies. Taking $E(M)$ as the ground state energy for a solid of M electrons, and $M = N$ then:

$$G = I(N) - A(N) = [E(N - 1) - E(N)] - [E(N) - E(N + 1)] \tag{2.47}$$

Where $I(N)$ the first ionization energy and $A(N)$ is the first electron affinity. Kohn Sham density functional theory is an exact approach to computing ground state energy and electron density of M interacting electrons in an external potential. For a solid, Kohn Sham theory produces a band structure, with a non-zero band gap

$$g = \epsilon^{LU} - \epsilon^{HO} \tag{2.48}$$

where LU is the lowest unoccupied and HO is highest occupied states[29].

2.1.9 GLLB-SC to Describe Band Gaps

GLLB-SC (solid correlation) replaces the energy density functional with another one more convenient for solids[30]. It is based on the GLLB-type exchange and PBEsol correlation. The computational costs needed for GLLB-SC are similar to those for GGA calculations. GLLB-SC works with an electron gas response potential resulting in a discontinuity that provides good quasiparticle band gaps to be compared with experiments. In exact DFT, the quasiparticle band gap of an N electron system, as was defined in eq 2.47 can also be written as

$$E_g = I(N) - A(N) = E_G^{KS} + \Delta_{xc} \tag{2.49}$$

where $E_G^{KS} = \varepsilon_{N+1} - \varepsilon_N$ is the KS band gap and Δ_{xc} is the derivative discontinuity. The total GLLB-SC potential is

$$v_{GLLB-SC}(\mathbf{r}) = 2\epsilon_{xc}^{PBEsol}(\mathbf{r}) + \sum_i^{occ} K_x \sqrt{\varepsilon_r - \varepsilon_i} \frac{|\psi_i(\mathbf{r})|^2}{n(\mathbf{r})} + v_{resp}^{PBEsol}(r) + \tag{2.50}$$

Normally, to implement this, is necessary the derivative of the total energy, however, since GLLB-SC does not have that expression, it has to be written by hand. The PAW potential consists of a smooth part inside the augmentation sphere. To obtain a enough smooth potential the expression is

$$v_{GLLB-SC}(\mathbf{r}) = 2\epsilon_x^{PBEsol}[n(\mathbf{r}), |\nabla n|^2](\mathbf{r}) + \sum_i^{val} K_G \sqrt{\epsilon_r - \epsilon_i} \frac{|\psi(\mathbf{r})|^2}{\sum_i^{val} |\psi_i(\mathbf{r})|^2} + v_c^{PBEsol}[n(\mathbf{r}), |\nabla n(\mathbf{r})|^2](\mathbf{r})$$

$$\tag{2.51}$$

which is equivalent to the GLLB-SC potential but is smooth inside the augmentation spheres. Nevertheless, this smooth potential requires augmentation sphere corrections to obtain a correct description to calculate the total PAW Hamiltonian[30]

$$u_{xc} = v_{xc}(\mathbf{r}) + \sum_a^{atoms} \sum_{ij} |p_i^a\rangle(\langle\phi_i^a|v_{xc}^a(\mathbf{r})|\phi_j^a\rangle - \langle\phi_i^a|v_{xc}^a(\mathbf{r})|\phi_j^a\rangle) \times \langle p_j^a| \tag{2.52}$$

2.2 Representations of the KS wavefunctions

DFT computations typically employ one of three forms to represent the KS wavefunctions, each one with its advantages: real space, plane waves (PWs), or linear combinations of atomic orbitals (LCAOs). In the real space representation approach, the wavefunctions are directly sampled at a finite number of grid points in real space. For the PW representation, the wavefunctions are expanded in terms of a basis set of plane waves. This representation is particularly common in periodic systems. Finally, in LCAO representation the wavefunctions are expanded in terms of a basis set consisting of linear combinations of atomic orbitals. This approach is often used in molecular systems and allows for a more localized description of the electronic structure.

A wavefunction lives in Hilbert space, which is a vector space with an inner product. States are shown as elements within this vector space, allowing them to be expressed as a linear combination of basis vectors. Additionally, any state ψ can be expressed as a linear combination of vectors of a complete basis set ϕ_μ.

$$\psi_n(\mathbf{r}) = \sum_\mu c_{n\mu}\phi_\mu(\mathbf{r}) \tag{2.53}$$

The basis set is used to expand the WF to find a solution to the KS equations. Even if it is possible to describe the real space and PW representations, only LCAO will be described more accurately since this is the method used to solve KS wavefunctions in this thesis.

2.2.1 Linear Combination of Atomic Orbitals

The linear combination of atomic orbitals (LCAO) is a technique for calculating molecular orbitals. It is possible to represent the KS wave functions using the assumption that the molecular orbitals can be constructed using a certain number of atomic orbitals. n atomic orbitals can be

combined to get n molecular orbitals.

$$\psi_n(\mathbf{r}) = \sum_\mu c_{n\mu}\Phi_\mu(\mathbf{r}) \tag{2.54}$$

where ψ_n represents the molecular orbital constructed by the atomic orbitals $\Phi_\mu(\mathbf{r})$, each one multiplied by its respective coefficient represented with n, and $\mu = (n, l, m)$. Then one gets the basis functions which are the products of numerical radial functions and spherical harmonics[31].

$$\Phi_{nml}(\mathbf{r}) = \Phi_{nml}(\mathbf{r}_a + \mathbf{R}_a) = \zeta_{nl}(\theta, \phi)Y_{lm}(\theta, \phi) \tag{2.55}$$

with $\mathbf{R}_a$ as the position of nucleus a, and $\mathbf{r}_a = \mathbf{r} - \mathbf{R}_a$

2.3   Green's Functions

The Green's functions are integrals that are used to solve ODE and PDE[32]. Mathematically, given a linear differential operator $L = L(x)$ acting on a subset Ω, the Green's function $G = G(x, x')$ at point $x' \in \Omega$ corresponding to L is any solution of

$$LG(x, x') = \delta(x - x') \tag{2.56}$$

Where x' are points such that $x' \in \Omega$. Then it is possible to multiply the last identity by a function $f(x')$ and integrate with respect to x'

$$\int LG(x, x')f(x')dx' = \int \delta(x - x')f(x)dx' = f(x) \tag{2.57}$$

Since L is a linear operator acting on x, the left hand side can be rewritten as

$$L\int (G(x, x')f(x')dx') \tag{2.58}$$

Therefore one can solve for $u = u(x)$ in differential equations of the form

$$Lu(x) = f(x) \tag{2.59}$$

so that

$$Lu(x) = L\left(\int G(x, x')f(x')dx'\right) \tag{2.60}$$

and finally $u(x)$ reduces to

$$u(x) = \int G(x, x')f(x')dx' \tag{2.61}$$

Considering the case of a two-point function, the problem of determining the potential $\psi(\mathbf{r})$ created by a charge distribution with a charge density $\rho(\mathbf{r})$, applying Poisson's equation[33] and Coulomb's law to the potential produced by each element of charge $\rho(\mathbf{r}')d^3\mathbf{r}'$ at $\mathbf{r}$ results in a solution

$$\psi(\mathbf{r}) = \frac{1}{4\pi\varepsilon_0} \int \frac{\rho(\mathbf{r}')}{|\mathbf{r} - \mathbf{r}'|} d^3\mathbf{r}' \tag{2.62}$$

which is consistent over the region $\rho(\mathbf{r}' \neq 0)$. Since the right-hand side can be treated as an operator that converts ρ into ψ, it is possible to write the solution in terms of Green's function

$$G(\mathbf{r}, \mathbf{r}') = \frac{1}{4\pi\varepsilon} \frac{1}{\mathbf{r} - \mathbf{r}'} \tag{2.63}$$

Finally, the integral becomes

$$\psi(\mathbf{r}) = \int G(\mathbf{r}, \mathbf{r}')\rho(\mathbf{r}')d^3\mathbf{r}' \tag{2.64}$$

Some authors prefer to denote the variables x and x' in terms of $\mathbf{r}$ and $\mathbf{r}'$. It is also common to find this definition with a negative sign, then G is defined as[34]

$$LG(x, x') = -\delta(x - x') \tag{2.65}$$

2.4 Non-Equilibrium Green's Functions

The non-equilibrium Green's functions (NEGF) provide a conceptual basis for the development of models for describing quantum transport. For the simulation of a device, it is necessary to perform a self-consistent solution for a transport equation and a Poisson equation. The transport equation calculates the electron density $n(\mathbf{r})$ and the current I for a given potential $U(\mathbf{r})$, at the same time the Poisson equation calculates the effective potential $U(\mathbf{r})$ that an electron feel due to the other electrons[35].

First of all, it is necessary to reach a Hamiltonian H capable of reproducing a good enough description of some device. When this device is connected to the contacts there is some charge

transfer in and out that produces a potential $U(r)$. Normally the potential $U(r)$ is calculated self consistently using the Schrödinger-Poisson solver for some electron density $n(r)$[36].

$$n(r) = \sum_{\alpha} |\Psi_{\alpha}(r)|^2 f_0(\epsilon_{\alpha} - \mu) \tag{2.66}$$

using the eigenstates $\Psi_{\alpha}(r)$ obtained from the Schrödinger equation

$$[H + U]\Psi_{\alpha}(r) = \epsilon_{\alpha}\Psi_{\alpha}(r) \tag{2.67}$$

and according to the Fermi function

$$f_0(E - \mu) = \frac{1}{1 + \exp[\frac{E-\mu}{k_B T}]} \tag{2.68}$$

If some device is connected to two contacts with different Fermi levels μ_1 and μ_2 the first goal is to obtain the electron density. Nevertheless, the density matrix $\rho_{\alpha\beta}$ has to be calculated before, since it has all the relevant physical quantities such as charge, current, energy current, etc.

$$n(r) = \sum_{\alpha\beta} \Psi_{\alpha}(r)\psi_{\beta}^*(r)\rho_{\alpha\beta} \tag{2.69}$$

In the so-called real space representation it is possible to write

$$[\rho]_{rs} = [V][\rho][V]^{\dagger} \tag{2.70}$$

With $[V]$ as a transformation matrix obtained from the wavefunctions Ψ_{α} at points r in real space

$$[V]_{r,\alpha} = \Psi_{\alpha}(r)\sqrt{\Omega} \tag{2.71}$$

finally obtaining

$$\rho(r, r') = \Omega \sum_{\alpha\beta} \Psi_{\alpha}(r)\Psi_{\beta}^*(r')\rho_{\alpha\beta} \tag{2.72}$$

which is an expression that can give us the density matrix of a device connected to two contacts with different Fermi levels. Then the density matrix is the electron density multiplied by a constant factor Ω which is the volume of the unit cell. The problem of finding the density matrix is more complex than only knowing $(H + U)$, also is necessary to realize how the scattering processes of the contacts are. This information can be obtained from the self-energy functions $\sum_1, \sum_2, \sum_s$.

With all of this information, it's possible to determine the density matrix and therefore the electron density and the current. The NEGF formalism can be applied to a large set of devices such as nanotubes or molecules[37].

The density matrix is given by:

$$\rho_k = \int \frac{dE}{2\pi} [f_0(E + \epsilon_k - \mu_1)A_1 + f_0(E + \epsilon_k - \mu_2)A_2] \tag{2.73}$$

with A_1 and A_2 being the left and right spectral functions respectively, defined by

$$A_1 = G\Gamma_1 G^+ \tag{2.74}$$

$$A_2 = G\Gamma_2 G^+ \tag{2.75}$$

and the associated Green's functions

$$G = [EI - HL - \Sigma_1 - \Sigma_2]^{-1} \tag{2.76}$$

and the gamma functions composed by the self-energy matrices,$\Sigma_{1,2}$, constructing a system in which the scattering processes are not included or coherent transport

$$\Gamma_{1,2} = [\Sigma_{1,2} - \Sigma_{1,2}^+] \tag{2.77}$$

Therefore, it is possible to find the current using

$$I = (-q)Trace(\rho J_{op}) \tag{2.78}$$

with J_{op} as the current operator.

$$[J_{op}] = (\frac{t}{\hbar N})\begin{bmatrix} 0 & -i & 0 & ... \\ +i & 0 & -i & ... \\ 0 & +i & 0 & ... \\ ... & ... & ... & ... \end{bmatrix} \tag{2.79}$$

Also it can be calculated the transmission by the following expression

$$I = (\frac{-q}{h}) \int dET(E)(F_1 - F_2) \tag{2.80}$$
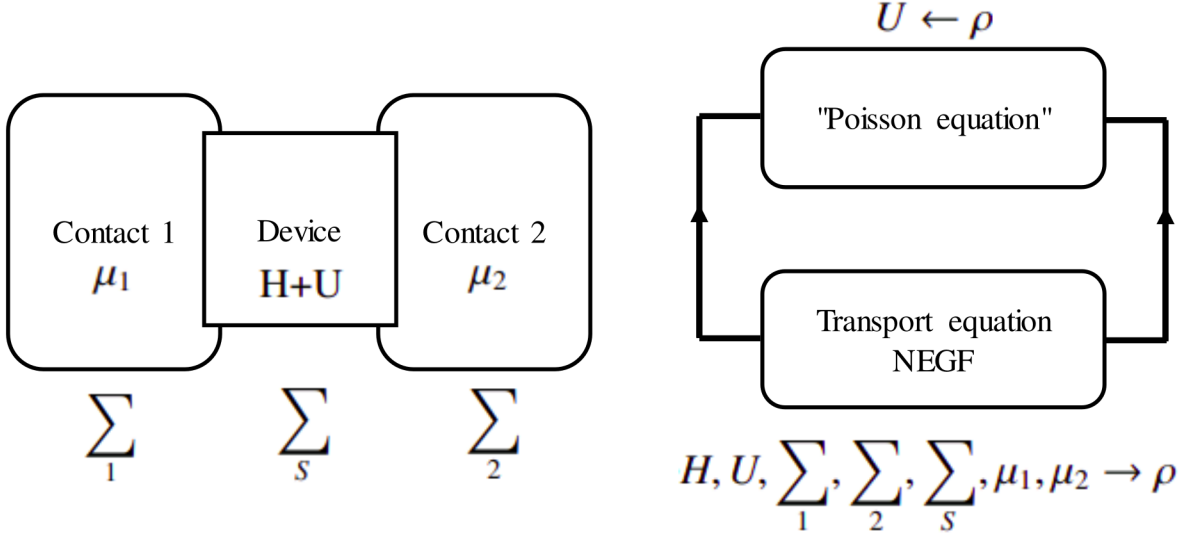
Figure 2.2: A: Two contacts connected to a device each one with its own Fermi level μ_1, μ_2 and self energies $\Sigma_1, \Sigma_2, \Sigma_s$. B: NEGF formalism self-consistent solver through Poisson equation. Adapted from ref[35].

where $T(E)$ is the probability of an electron transmitting from the left to the right contact. Additionally, F_1 and F_2 can be written as

$$F_1 = F_0(E - \mu_1) \tag{2.81}$$

$$F_2 = F_0(E - \mu_2) \tag{2.82}$$

with F_0 being the logarithmic function that replaces the Fermi function f_0.

The NEGF formalism can be used to evaluate the transmission probability, nevertheless, the true using of this formalism lies in describing this kind of system, including scattering processes, or what is called the non-coherent transport.

As it is shown in Figure 2.2, the self-energy function Σ_s represents the scattering processes of the NEGF formalism. Taking into account that the Σ_s is dependent on the density matrix and has to be calculated self consistently, the NEGF formalism gives a clear description to calculate Σ_s. Therefore, this description can be used to develop the research of physical descriptions of energy distributions in nanoscale devices. The scattering process can be viewed as another contact

described by Σ_s additional to the self energies of the contacts 1 and 2 described by Σ_1 and Σ_2 respectively. Then it can be included as

$$G = [EI - H - \Sigma_1 - \Sigma_2 - \Sigma_s]^{-1} \tag{2.83}$$

$$\Gamma_{1,2,s} = i[\Sigma_{1,2,s} - \Sigma_{1,2,s}^+] \tag{2.84}$$

$$A_1 = G\Gamma_1 G^+, A_2 = G\Gamma_2 G^+, A_s = G\Gamma_s G^+ \tag{2.85}$$

Then the matrix can be written as

$$\Sigma_s = \begin{bmatrix} \eta_1, 0, 0, ... \\ 0, \eta_2, 0, ... \\ 0, 0, \eta_3, ... \\ ..., ..., ..., ... \end{bmatrix} \tag{2.86}$$

where η represents the phenomenological parameters related to the scattering time τ by $\tau = \frac{\hbar}{2\eta}$. Nevertheless, the scattering contact Σ is not a "contact" itself, therefore it does not have a well-defined Fermi level μ_s that can be used to calculate F_s. Because of this, it is constructed a more physically correct model in which each lattice "n" has a different μ_{s_n}, that will be named as in scattering function[36]:

$$\Sigma_s^{in} = \begin{bmatrix} F_{s1}\eta_1, 0, 0, ... \\ 0, F_{s2}\eta_2, 0, ... \\ 0, 0, F_{s3}\eta_3, ... \\ ..., ..., ..., ... \end{bmatrix} \tag{2.87}$$

Then one calculates the density matrix from

$$2\pi[\rho(E)] = F_1 A_1 + F_2 A_2 + G\Sigma_S^{in} G^+ \tag{2.88}$$

2.5   Projector augmented wave method

The projector-augmented wave method is a technique to perform electronic structure calculations. The features of the wave functions are different at each region of the space. In the bonding region, the wave functions are smooth, however, at regions near nuclei wave functions have rapid oscillations due to the nucleus's attraction potentials. The procedure of the augmented wave

method is to divide the wave functions into parts called partial waves.[9] To solve this problem is introduced a linear transformation $\tilde{\mathcal{T}}$ which is used to go from smooth wave functions $|\tilde{\psi}_n\rangle$ to the all-electron Kohn-Sham single particle wave functions $|\psi_n\rangle$ such as:

$$|\psi_n\rangle = \tilde{\mathcal{T}}|\tilde{\psi}_n\rangle \tag{2.89}$$

with n being the quantum state label. Then the transformed Kohn-Sham equations have to be solved.

$$\tilde{\mathcal{T}}^\dagger \tilde{H} \tilde{T} |\tilde{\psi}_n\rangle = \epsilon_n \tilde{\mathcal{T}}^\dagger \tilde{\mathcal{T}} |\tilde{\psi}_n \tag{2.90}$$

Now it is needed to define $\tilde{\mathcal{T}}$ in such a way that wave fucntions $|\tilde{\psi}_n\rangle$ becomes smooth. Taking advantage of $|\psi_n\rangle$ are already smooth at a certain distance from the core, $\tilde{\mathcal{T}}$ only modify WF close to nuclei.

$$\tilde{\mathcal{T}} 1 + \sum_a \tilde{\mathcal{T}}^a \tag{2.91}$$

with $\tilde{\mathcal{T}}^a$ having no effect outside a certain region $|\mathbf{r} - \mathbf{R}^a| < \mathbf{r}^a_c$. Here the $\mathbf{r}^a_c$ or cut-off radii have to be chosen in such a way that there is no overlap in the augmentation spheres. The true WF can be expanded into partial waves ϕ_i^a with it corresponding auxiliary smooth partial wave $\tilde{\phi}_i^{a\,38}$ requiring that

$$|\phi_i^a\rangle = (1 + \tilde{\mathcal{T}}^a)|\tilde{\phi}_i^a\rangle \Leftrightarrow \tilde{\mathcal{T}}^a|\tilde{\phi}_i^a\rangle = |\phi_i^a\rangle - |\tilde{\phi}_i^a\rangle \tag{2.92}$$

From eq 2.67 it's required the partial and smooth counterpart waves are equivalent outside the augmentation sphere

$$\forall a, \phi_i^a = \tilde{\phi}_i^a(r), > r_c^a \tag{2.93}$$

Hence the smooth all electron wave functions are expanded as

$$|\tilde{\psi}_n\rangle = \sum_i P_{ni}^a |\tilde{\phi}_i^a \tag{2.94}$$

where $|P_{ni}^a$ are the smooth projector functions treated as expansion coefficients. Using the fact that $|\psi_i^a\rangle = \tilde{\mathcal{T}}|\tilde{\psi}_i^a\rangle$ then the expansion

$$|\psi_n\rangle = \tilde{\mathcal{T}}|\tilde{\psi}_i^a\rangle = \sum_i P_{ni}^a |\phi_i^a\rangle \tag{2.95}$$

The expansion coefficients P_{ni}^a have to be linear functionals of $|\tilde{\phi}_n\rangle$ i.e.

$$P_{ni}^a = \langle \tilde{p}_i^a | \tilde{\psi}_n \rangle = \int d\mathbf{r}\, \tilde{p}_i^{a*}(r - R^a)\tilde{\psi}_n(\mathbf{r}) \tag{2.96}$$

where $|p_i^a\rangle$ are smooth projector functions inside the augmentation sphere which must satisfy.

$$\sum_i |\tilde{\psi}\rangle_i^a \langle \tilde{p}_i^a| = 1 \tag{2.97}$$

Also implies that

$$\langle \tilde{p}_{i1}^a | \tilde{\psi}_{i2}^a \rangle = \delta_{i1,i2} \tag{2.98}$$

By eq 2.72 the linear transformation becomes

$$\tilde{\mathcal{T}}^a = \sum_i \tilde{\mathcal{T}}^a |\tilde{\phi}_i^a\rangle\langle \tilde{p}_i^a| = \sum_i (|\phi_i^a\rangle - \langle \tilde{\phi}_i^a|)\langle \tilde{p}_i^a| \tag{2.99}$$

then by eq 2.66

$$\tilde{\mathcal{T}} = 1 + \sum_a \sum_i (|\phi_i^a\rangle - |\tilde{\phi}_i^a\rangle)\langle p_i^a| \tag{2.100}$$

Therefore we obtain the all-electron Kohn Sham WF $\psi_n(\mathbf{r})$ from

$$\psi_n(\mathbf{r}) = \tilde{\psi}_n(\mathbf{r}) + \sum_a \sum_i (\phi_i^a(\mathbf{r}) - \tilde{\phi_i^a}(\mathbf{r}))\langle \tilde{p}_i^a | \tilde{\psi}_n \rangle \tag{2.101}$$

The pseudo-wave functions are smoother and describe the core electrons and nuclei accurately.

Chapter 3

Methodology

*

3.1   External Quantum Efficiency calculation

As defined in the introduction part, the EQE can be defined as the ratio of excited and transmitted electrons N_e to incident photons N_ω at a certain energy $\hbar\omega$[39], then EQE can be written as

$$\eta_{EQE} = \frac{N_e}{N_\omega} \tag{3.1}$$

Is the probability of an electron at initial energy ε_i is exited by a photon to an energy $\varepsilon_f = \varepsilon_i + \hbar\omega$. Here η_{EQE} can be also defined as.

$$\eta_{EQE} = \int T(\varepsilon, \hbar\omega) p(\varepsilon, \hbar\omega) d\varepsilon \tag{3.2}$$

T is the absorption and transmission probability and p is the probability distribution of excitable electrons, where p can be defined as:

$$p(\varepsilon) = f(\varepsilon)(1 - f(\varepsilon + \hbar\omega))\varrho(\varepsilon) \tag{3.3}$$

---

*This work is based on the project in collaboration with Duncan J. Mowbray, Jeyson P. Alomoto-Catota, Daniel E. Gonzalez-Tamayo, and Vito Despoja, "Photoinduced Quantum Transport" (in progress 2024).

where ϱ_d is the density of normalized electronic states and f is the Fermi filling. As $f(\varepsilon)$ describes the fermi dirac distribution, the product $f(\varepsilon)(1 - f(\varepsilon + \hbar\omega))$ behaves as a Hevisae step function such that:

$$\int_{-\infty}^{\infty} p(\varepsilon\hbar\omega)d\varepsilon = \int_{-\hbar\omega}^{0} \varrho(\varepsilon)d\varepsilon = 1 \tag{3.4}$$

with all the energies referenced to the Fermi level ε_F. Then the only permitted transitions are from occupied to unoccupied states, which are given per unit photon of energy $\hbar\omega$. Now eq 3.2 can be expressed as:

$$\eta_{EQE} = \int_{\hbar\omega}^{0} T(\varepsilon, \hbar\omega)\varrho(\epsilon)d\varepsilon \tag{3.5}$$

The non-equilibrium Green's functions (NEGF) states that the probability of transmission of an electron through some region via appropriate eigenchannel of the transmission matrix $\mathcal{T}$ is given by the magnitude of its related eigenvalue $|\tau|_n$ [40][36]. Since the transmission between different eigenchannels acts in parallel, the conductance G is given by the sum of the eigenvalues scaled by the quantum conductance G_0, such that

$$G = G_0 \sum_{n=1}^{N} |\tau_n| \tag{3.6}$$

where N is the number of basis functions in the interface. To state the restriction that a photon can be absorbed only once, the probability for the excitation process is redefined as

$$T = 1 - \prod_{n=1}^{N}(1 - |\tau_n|) \tag{3.7}$$

and now $\mathcal{T}$ combines the absorption and transmission processes. The transmission matrix $\mathcal{T}$ can be defined as

$$\mathcal{T} = \mathcal{G}(\varepsilon, \hbar\omega)\Gamma_{in}(\varepsilon)\mathcal{G}^{\dagger}(\varepsilon, \hbar\omega)\Gamma_{out}(\varepsilon + \hbar\omega \tag{3.8}$$

with $\mathcal{G}$ is the Greens function of the interfacial region and Γ_{in}, Γ_{out} are the couplings to the input and output leads. Defining

$$\tilde{\varepsilon} = \varepsilon + i0^{+} \tag{3.9}$$

as the shift of the energy off the real axis $\mathcal{G}$ given by

$$\mathcal{G} = \begin{bmatrix} \tilde{\varepsilon}\mathcal{S} - \mathcal{H} - \Sigma_{in}(\tilde{\varepsilon}) & \mathcal{A}(\hbar\omega) \\ \mathcal{A}^{\dagger}(\hbar\omega) & (\tilde{\varepsilon} + \hbar\omega)\mathcal{S} - \mathcal{H} - \Sigma_{out}(\tilde{\varepsilon} + \hbar\omega) \end{bmatrix}^{-1} \tag{3.10}$$

with $\mathcal{A}$ is the coupling between occupied and unoccupied states via external electromagnetic fields, $\mathcal{S}$ and $\mathcal{H}$ are the overlap and Kohn Sham Hamiltonian matrices respectively, and $\Sigma_{in/out}$ are the self energies of the input and output leads. The coupling between input and output leads can be expressed in terms of the self-energies as

$$\Gamma_{in/out} = i(\Sigma_{in/out} - \Sigma_{in/out}^{\dagger}) \tag{3.11}$$

The self-energy of lead α is given by

$$\Sigma_\alpha(\tilde{\varepsilon}) = [\tilde{\varepsilon}S_{I\alpha} - \mathcal{V}_{I\alpha}][\tilde{\varepsilon}S_\alpha - H_\alpha]^{-1}[\tilde{\varepsilon}S_{I\alpha}^{\dagger} - \mathcal{V}_{I\alpha}^{\dagger}] \tag{3.12}$$

with S_α and H_α are the overlap and Hamiltonian matrices of lead α, $S_{I\alpha}$ and $\mathcal{V}_{I\alpha}$ are the overlap and coupling matrices of the interfacial region[41]. All matrices are represented using LCAO basis set, φ, indexed over a^{th} of N_{at} spatially ordered atoms and its ith of N_a basis functions, then $\mu = a, i$. Therefore, the overlap and Hamiltonian matrices are written as

$$\mathcal{S}_{\mu\nu} = \langle \varphi_\mu | \varphi_{nu} \rangle \tag{3.13}$$

and

$$\mathcal{H}_{\mu\nu} = \langle \varphi_\mu | \hat{H}_{ks}(\mathbf{r}) | \varphi_\nu \rangle \tag{3.14}$$

The Kohn Sham Hamiltonian operator is defined as

$$\hat{\mathcal{H}}_{KS}(\mathbf{r}) = -\frac{\hbar^2}{2m_e}\nabla_{\mathbf{r}}^2 + V_H[\rho(\mathbf{r})] + V_{xc}[\rho(\mathbf{r})] + V_{ext}(\mathbf{r}) \tag{3.15}$$

with $\rho(\mathbf{r})$ as the electron density, $V_H[\rho(\mathbf{r})]$ as the Hartree potential, $V_{xc}[\rho(\mathbf{r})]$ is the exchange correlation potential and $V_{ext}(\mathbf{r})$ is the external potential due to environment.

Furthermore, the coupling between occupied and unoccupied states via photon absorption is defined as

$$\mathcal{A}_{\mu\nu} = \langle \varphi_\mu | \hat{\mathcal{A}}(\mathbf{r}, t) | \varphi_\nu \rangle \tag{3.16}$$

as depicted schematically in Figure 3.1, the operator $\hat{\mathcal{A}}$ is defined as the time-dependent interaction with an external electromagnetic field and is written

$$\hat{\mathcal{A}}(\mathbf{r}, t) = \frac{e}{2mc}(\hat{\mathbf{A}} \cdot \hat{\mathbf{p}}) = -i\frac{e\hbar}{2mc}\mathbf{A}(\mathbf{r}, t) \cdot \nabla_r \tag{3.17}$$
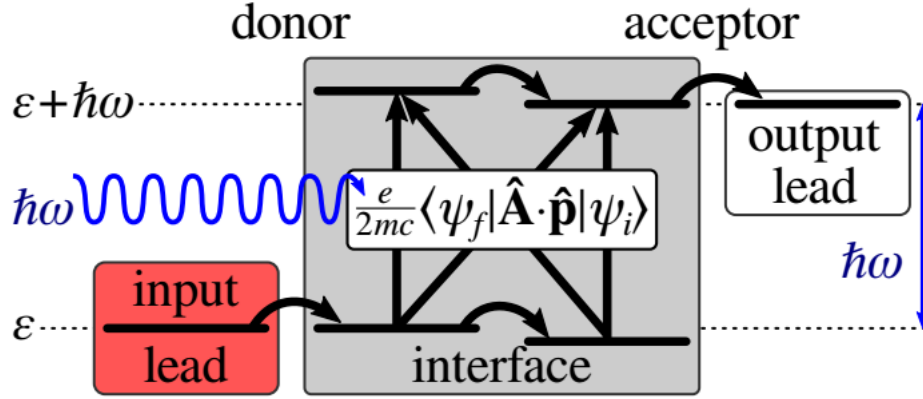
Figure 3.1: Schematic of an excitation process across a donor–acceptor interface from an occupied initial state with energy ε_i in the input lead to an unoccupied intermediate state with energy $\varepsilon_i + \hbar\omega$ via the interaction between an external electromagnetic field with vector potential $\hat{\mathbf{A}}$ and momenta $\hat{\mathbf{p}}$, and via coupling to a phonon mode of energy hv to an unoccupied final state with energy $\varepsilon_f = \varepsilon_i + \hbar\omega - hv$ in the output lead.

is the time-dependent interaction with external electromagnetic field taken to first order in vector potential $\mathbf{A}(\mathbf{r}, t)$ in the coulomb gauge $\nabla \cdot \mathbf{A} = 0$. Noting that $\frac{e\hbar}{2mc} \approx \frac{1}{274}$ in atomic units, justify that $\hat{\mathbf{A}}(\mathbf{r}, t)$ can be treated as a perturbation of $\hat{\mathcal{H}}_{KS}(\mathbf{r})$. The vector potential of a spherical electromagnetic wave in vacuum takes the form

$$\mathbf{A}(\mathbf{r}, t) = A_0 sin(kr - \omega t)\hat{\mathbf{e}}_{\mathbf{q}} \tag{3.18}$$

where $k = \omega/c$ and $\hat{\mathbf{e}}_{\mathbf{q}}$ is the field's polarization direction. The time-averaged energy density stored in this field is $\langle u_{em} \rangle_t = \epsilon_0 c \omega^2 A_0^2/2$. The energy density field is the product of the photon density ρ_ω and their energy $\hbar\omega$, i.e., $u_e m = \rho_\omega \hbar\omega$. Equating the classical and quantum mechanical energy density we can describe the magnitude of the vector potential A_0 in terms of the photon frequency ω such as

$$A_0 = \sqrt{\frac{2\hbar\varrho_\omega}{\epsilon_0\omega}} \tag{3.19}$$

Since η_{EQE} is defined per incident photon, $\rho\omega = \frac{1}{\Omega}$ where Ω is the volume of the unit cell, obtaining $A_0 = \sqrt{\frac{8\pi}{\Omega\omega}}$ in atomic units. The matrix elements for the coupling between initial and

intermediate states are

$$\mathcal{A}_{\mu v} = -i \frac{e\hbar^2}{2m} \sqrt{\frac{\mu_0}{2\Omega\hbar\omega}} \hat{\mathbf{e}}_q \cdot \langle \varphi_\mu | \nabla | \varphi_v \rangle \tag{3.20}$$

3.2 Computational details

The DFT calculations of the PCBM[21] system were performed using the GPAW[42] implementation as well as the ASE[10] packages over our EQE Python code[43]. There was created an array of two PCBM molecules which were treated through the use of a relaxation process using a Grimme's semi- empirical D3[44] approach. The ASE calculator DFT-D3 is used because it is needed to take into account the van der Waals interactions between the molecules. Also, the double-zeta polarized (dzp) basis set of LCAO[45] is used to represent KS wavefunctions and electron density. This first step reaches the minimum energy configuration of the system by iterative adjusting the positions of atoms, relaxing the potential energy until the maximum force is less than 0.03 eV/Å. The relaxation process finished with a minimized unit cell of $(25.6 \ x \ 28.8 \ x \ 25.6)Å^3$ in the x, y, and z directions respectively.

The exchanging correlation potential of GLLB-sc provides an explicit analytical form for the derivative discontinuity correction so it is easy to compute. We use the derivative discontinuity correction to shift the khon sham energy gap that we get from PBE correlation potential Δxc[46][47].

Then, the external quantum efficiency and transmission probabilities were calculated considering the occupied and unoccupied states. For those calculations, we used a broadening of 25μeV for the calculation of the density of states.

Chapter 4

Results & Discussion

This chapter is structured into six sections. The first section presents the minimum energy result from the relaxation process. The second subsection presents the EQE calculations for the PCBM molecule with light polarization in the *x*-direction and the transmission. The third shows the results corresponding to the EQE calculation of the PCBM with light polarized in the *y*-direction, and transmission. The fourth section explains the results of EQE of PCBM with light polarized in the *z*-direction, and transmission. The fifth section discusses how is the transmission and efficiency behavior for an arrangement of 4 PCBMs with light polarized in *z*-direction. Finally, the sixth section discusses about the excitonic density HUMO and LUMO wavefunctions of the PCBM.

4.1 Relaxed cell, EQE results for 2PCBMs polarized in *x*, *y*, and *z*, 4 PCBMs polarized in *z*-direction and HOMO-LUMO wavefunctions

4.1.1 Relaxed PCBM unit cell results

Figure 4.1 shows the energy change in electron volts (eV) versus the distance in Å of the PCBM unit cell. In this way, we determine the most stable configuration for a periodic chain of the PCBM molecule's unit cell based on its minimum energy. The code used to obtain this
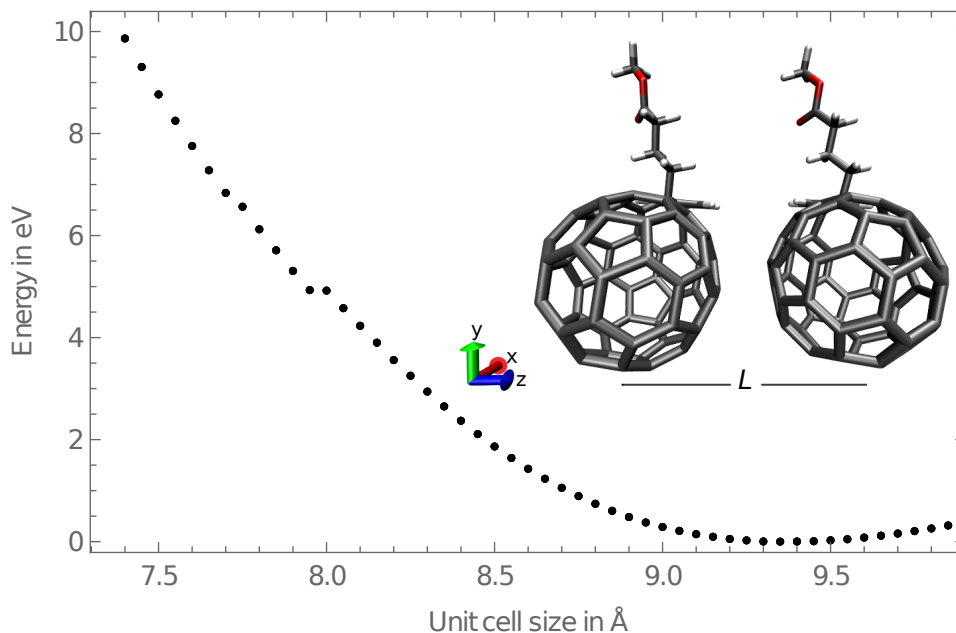
Figure 4.1: Energy in eV vs PCBM separation in Å. The minimum value of the energy corresponds to the most stable configuration and minimized PCBM unit cell system along the z direction. L represents the distance at which the energy is minimum from center to center.

plot uses an arrangement of two PCBM molecules which will be approaching each other in z direction measuring the energy at each step. The performed calculation runs based on GPAW implementation code using PBE exchange-correlation functional, 680 bands, a configuration of [128, 144, 192] grid points, a structure of [1, 1, 5] k-points, and a Fermi-Dirac electronic temperature of $k_B T = 25$ meV. As the separation between PCBMs decreases, the energies tend to diminish because of the attractive van der Waals forces between the two PCBM molecules. The trend reaches a point where the energy has a minimum value and then tends to increase as the PCBMs get even closer, meaning that electrostatic repulsion now dominates. It can be noted that the minimum energy configuration for the size of the unit cell corresponds to 9.35Å. This is the most stable configuration that will be used for the subsequent calculations.

The resulting atomic structure was used to calculate the electronic density, wavefunctions, derivative discontinuity correction, Hamiltonian, and overlap matrices, that will be used as input to our EQE calculations.

We obtain a derivative discontinuity correction of 0.577 eV, yielding a band gap of 1.88 eV. After that, both the derivative discontinuity correction and the corresponding most stable unit cell were used to perform the EQE calculation, the density of occupied and unoccupied states, and transmission probabilities. Finally, there were made calculations for 2PCBMs which use one PCBM as two principal layers, in this way, we are taking into account all the interactions between the left-hand side and the right-hand side of the molecule but dropping out all the interactions with the neighboring molecule. Also we performed the calculation using 4PCBMs. In this case, we are heating one PCBM as one principal layer considering all the interactions between one PCBM and its neighbor but zero interactions with a third PCBM.

4.1.2   **PCBM with light polarized in *x*-direction**

Figure 4.2 shows a schematic of the whole EQE calculation process: Fig. 4.2 a) shows the occupied DOS in arbitrary units versus the energy from 0 to 4 eV; Fig. 4.2 b) shows the unoccupied DOS in arbitrary units versus the energy from -4 to 0 eV; Fig. 4.2 c) is the absorption and transmission probability T as function of initial energy ε_i and excitation energy $\hbar\omega$ in eV; Fig. 4.2 d) shows the external quantum efficiency η_{EQE} versus the excitation energy $\hbar\omega$ from 0 to 4 eV;. The white dashed lines mark the top and bottom of each energy band of the occupied and unoccupied DOS. It can be noticed that there exist three principal regions of available allowed states for absorption to occur. The first one appears due to the overlapping of the first Lowest unoccupied molecular orbital (LUMO) and highest occupied molecular orbital (HOMO) states, has the smallest transmission of the three regions, and is related to the EQE structure around 1.8 and 2.4 eV. The second one comes from the overlapping of the second LUMO and first HOMO states and has few structures where the transmission can occur and is related to the EQE structure at 4 eV. The third one arises from the first LUMO and second HOMO states and has a larger transmission structure, which will give a more important contribution to the EQE probability and is related to the EQE structure around 2.8 and 3.8 eV. The transmission color bar indicates the percentage of the incoming photons that will become charge carriers according to the colors of the overlapping regions.

Discussing Fig. 4.2 d) in deep, we have isolated molecular states that broaden into "bands" due to overlap between the neighboring PCBM molecules. It can be noted that there exist three principal regions where the exited electrons can jump. The first structure can be found around
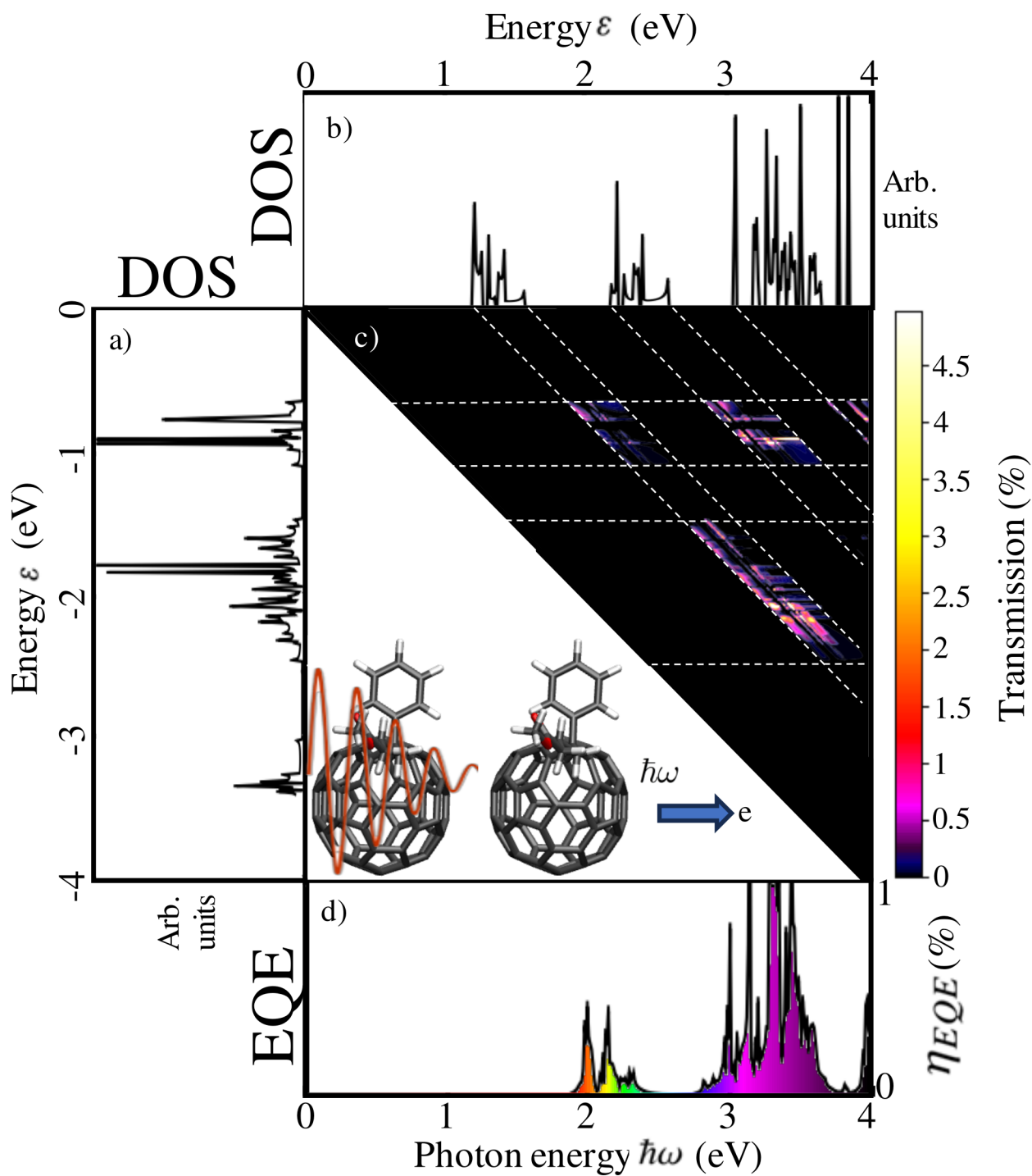
Figure 4.2: a) The occupied DOS in arbitrary units plotted from 0 to 4eV; b) unoccupied DOS plotted from 0 to -4eV; c) transmission probabilities from 0 to 5%, d) EQE probability for light polarization in the x direction for photon energies from 0 to 4eV.

1.8 and 2.4eV, this means that it is possible to get some electrons with energy that corresponds to a small part of the visible range. The second structure corresponds to a part of the visible spectra and a small part of the ultraviolet, it is around 2.8 and 3.8 eV and has the majority of the excited electrons. This part generates the largest contribution of the charge carriers of the system. The last EQE structure is around 4eV which corresponds to the ultraviolet region and represents the smallest contribution of the EQE that can generate charge carriers. There also exists a reasonably large energy difference between the first and second structure that separates low and high-energy charge carriers. Therefore, due to the molecular nature of the system, the exited electrons tend to stay in the second EQE structure around 2.8 - 3.8eV. In other words, charge carriers are more long-lived in those high-energy states, making it easier to harness the energy of high-energy UV photons. Molecular electronics allows us to have discrete energy levels so that in the same system, it is possible to excite electrons to different energies and use that higher voltage to do work. In common systems such as silicon, the band gap can be modeled as the difference between the valence band maximum and conduction band minimum transition. Nevertheless, PCBM is a molecule and therefore does not have its molecular states broadened into bands. This means for an excited electron in some unoccupied state there will be no overlap with the valence band maximum. It means that LUMO and LUMO+2 will not overlap.

4.1.3 PCBM with light polarized in the *y*-direction

Figure 4.3 shows a schematic of the whole EQE calculation process with light polarized in y direction, Fig. 4.3 a) represents the occupied DOS in arbitrary units versus the energy from 0 to 4eV; Fig. 4.3 b) represents the unoccupied DOS in arbitrary units versus the energy from -4 to 0eV; Fig. 4.3 c) is the absorption and transmission probability T as a function of initial energy ε_i and excitation energy $\hbar\omega$ in eV; Fig. 4.3 d) represents the external quantum efficiency η_{EQE} versus the excitation energy $\hbar\omega$ from 0 to 4eV.

Anew, the white dashed lines mark the top and bottom of each energy band of the occupied and unoccupied DOS. Also, there exist the same three principal regions of available allowed states for absorption to occur, nevertheless, the colors and structures in the transmission plot are a bit different due to the change in polarization. Similarly, the first region appears due to the overlapping of the first LUMO and HOMO states, has the smallest transmission, and is related to the small structure around 2.2eV. The second one comes from the overlapping of the second
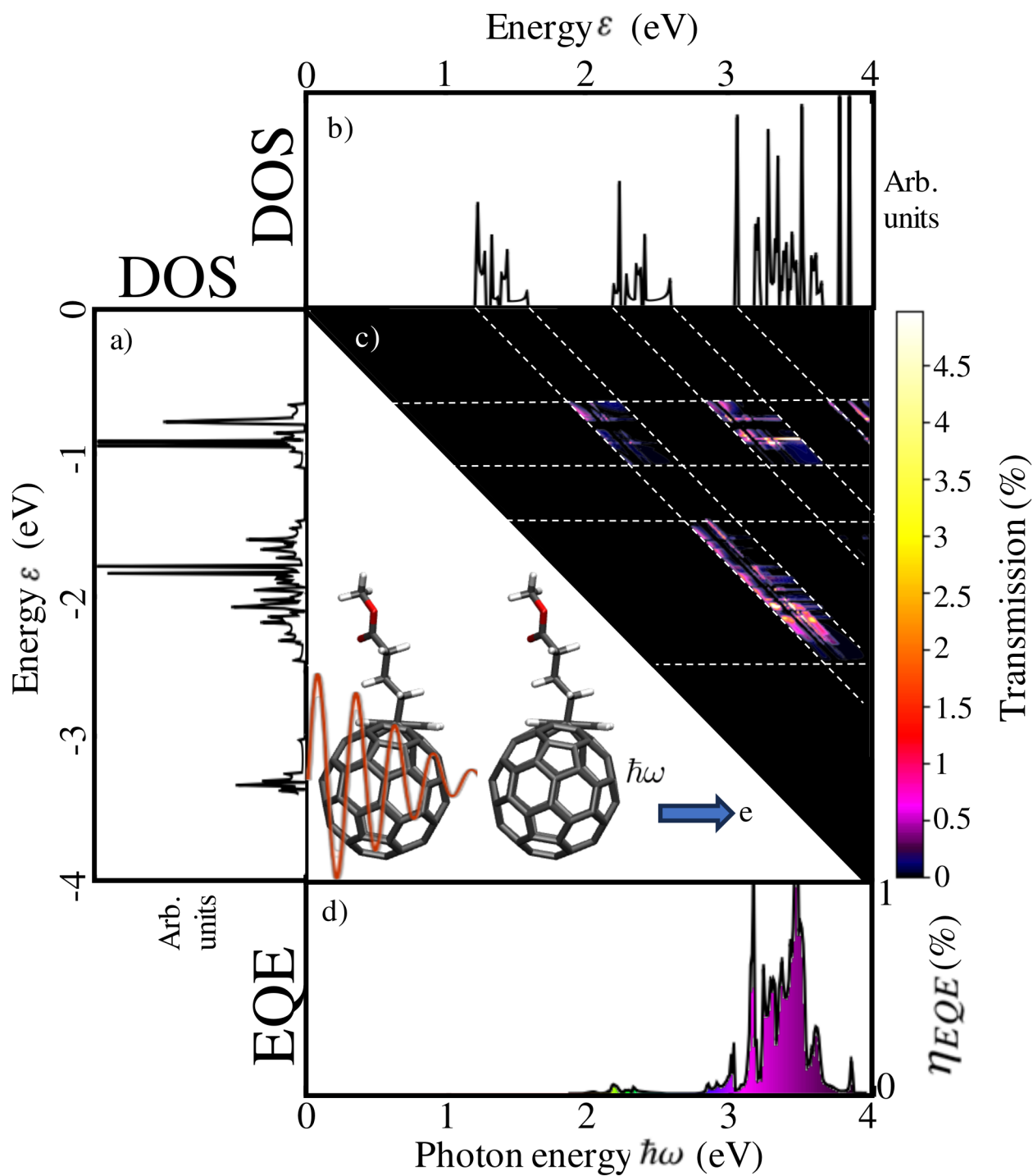
Figure 4.3: a) The occupied DOS in arbitrary units plotted from 0 to 4eV; b) unoccupied DOS in arbitrary units plotted from 0 to -4eV; c) transmission probabilities from 0 to 5%; c) EQE probability with light polarization in the *y*-direction for photon energies from 0 to 4eV.

LUMO and first HOMO states, it has few structures where the transmission can occur and is related to the EQE structure at 4eV. The third one arises from the first LUMO and second HOMO and has a larger transmission structure, which will give a more important contribution to the EQE probability and is related to the EQE structure around 2.8 and 3.8eV. The transmission color bar indicates the percentage of the incoming photons that will become charge carriers according to the colors of the overlapping regions.

Explaining Fig. 4.3 d) in deep, there exist three regions where exited electrons can be stored. Nevertheless, the first around 2eV and the third one around 4eV are too small, and almost no electrons can be exited at those energies. The most important EQE region where the exited electrons can jump lies around 2.8 and 3.8eV. This means that the electrons that remain in that region will generate the majority of charge carriers of the system. It is possible to find the same band gap that appears in Figure 4.4 between the first and second structures. Therefore, the electrons are more long-lived in the high-energy states of the second structure.

4.1.4 PCBM with light polarized in the *z*-direction.

Figure 4.4 shows a schematic of the whole EQE calculation process with light polarized in the *z*-direction, Fig. 4.4 a) represents the occupied DOS in arbitrary units versus the energy from 0 to 4eV; Fig. 4.4 b) represents the unoccupied DOS in arbitrary units versus the energy from -4 to 0eV; Fig. 4.4 c) is the absorption and transmission probability T as a function of initial energy ε_i and excitation energy $\hbar\omega$ in eV; Fig. 4.4 d) represents the external quantum efficiency η_{EQE} versus the excitation energy $\hbar\omega$ from 0 to 4eV.

Anew, the white dashed lines mark the top and bottom of each energy band of the occupied and unoccupied DOS with the same three principal regions of available allowed states for absorption to occur. Again, the colors and structures in the transmission plot are a bit different due to the light polarization in *z*. The first region appears due to the overlapping of the first LUMO and first HOMO states, has the smallest transmission, and is related to the small structure around 1.8 and 2.4eV. The second one comes from the overlapping of the second LUMO and first HOMO states, it has few structures where the transmission can occur and is related to the EQE structure at 4eV. The third one arises from the first LUMO and second HOMO states and has a larger transmission structure, which will give a more important contribution to the EQE probability and is related to the EQE structure around 2.8 and 3.8eV. The transmission color bar indicates the percentage of
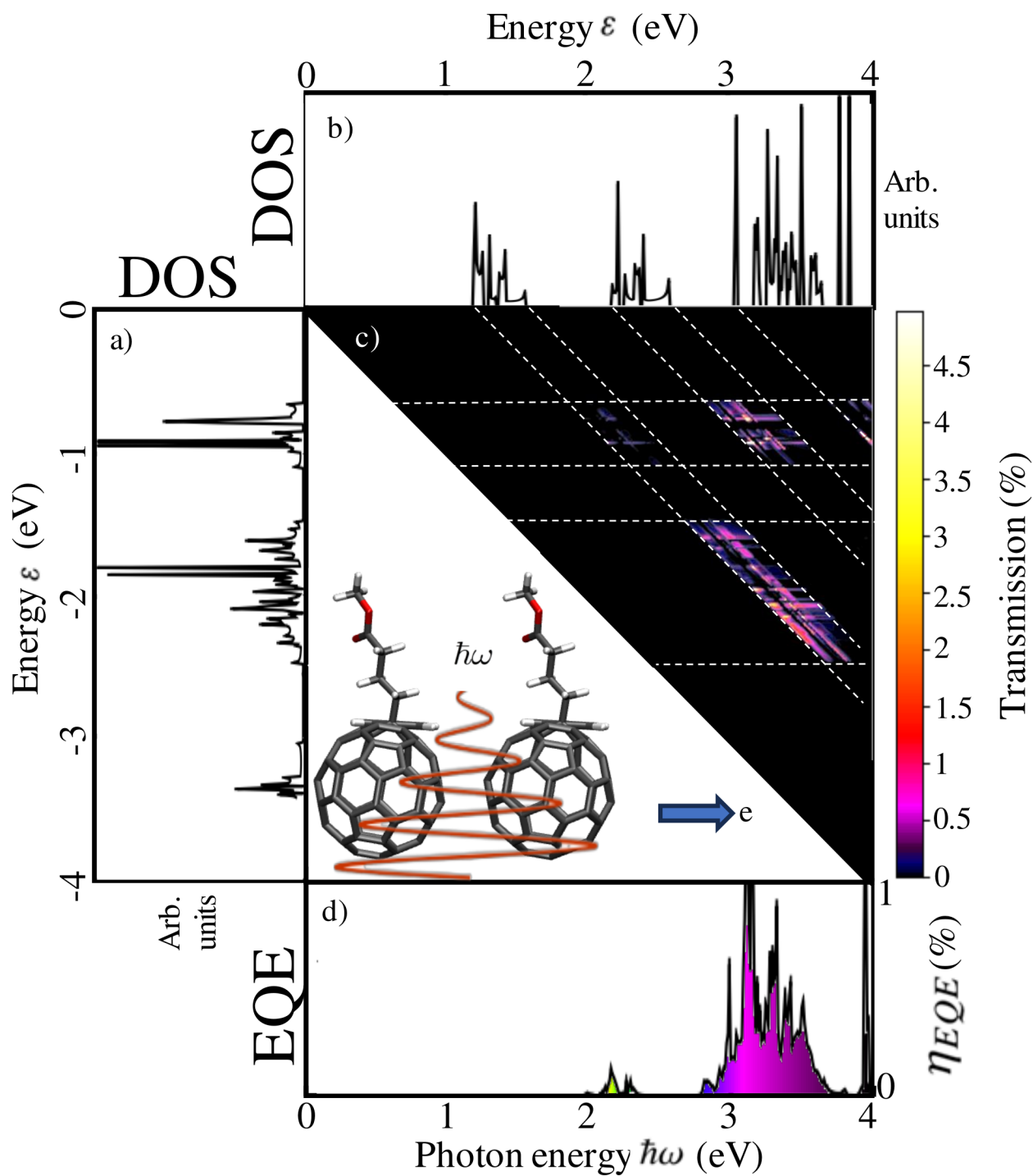
Figure 4.4: a) The occupied DOS in arbitrary units plotted from 0 to 4eV; b) unoccupied DOS in arbitrary units plotted from 0 to -4eV; d) transmission probabilities from 0 to 5%; c) EQE probability with light polarization in the *z*-direction for photon energies from 0 to 4eV.

the incoming photons that will become charge carriers according to the colors of the overlapping regions.

Explaining Fig. 4.4 d) more accurately, there exist three regions where exited electrons can be stored. There exist some small peaks around 2eV and a sharp peak around 4eV, then some electrons can be exited at that energies, but the most important EQE region where exited electrons can jump lies around 2.8 and 3.8eV. This means that the remaining electrons in that region will generate the majority of charge carriers of the system. Again, it is possible to find an energy separation that appears in Fig. 4.4 d) and Fig. 4.6 d) between the first states around 2eV and the second states around 3eV. Therefore, the electrons are more long-lived in the high-energy states of the second structure.

One interesting remark is that if we analyze the figures 4.2 d), 4.3 d) and 4.2 d) the resulting EQE in the *y* and *z*-directions has a few states around 2ev, in comparison with the *x*-direction which is the one that has more states at that region of the visible spectra. This can be explained by the relative facility for an electron to do a transition according to the direction. With the light polarized in the *x*-direction, an electron can jump more easily from the functional group to the fullerene, and it is reflected with more states around 2eV in the EQE plot. For light polarized in the *y*-direction, the transitions can also occur from the functional group to the fullerene, nevertheless is less efficient compared with polarization in *x*. In contrast, for *z*-polarization the electrons excite from the fullerene to the neighboring fullerene, therefore the excitations will be reduced due to the separation distance. This is reasonable since the polarization in *z* has the lowest EQE states for high-energy photons around 3 and 4eV.

Finally, it is necessary to mention that in solution, the PCBM molecules are oriented randomly, to model this computationally we are creating a semi-infinite arrangement of PCBM molecules oriented the same to simplify the problem. We expect that the results we obtain by doing this approximation do not affect the efficiency results appreciably because as we can see in fig 4.6 in the transitions only participate the fullerene.

4.1.5 4PCBM with light polarized in the *z*-direction.

In Fig. 4.5 we can see that the occupied density of states is slightly different compared to its counterpart with a unit cell of 2 PCBM molecules. Also, the transmission color structure and the EQE change a bit. We can see an increase in the probability states around the visible spectra. This

information tells us that including all the atomic interactions using a 4 PCBM unit cell increases the probability of a photon being absorbed and transmitted. Additionally, with all these examples, we can infer that the model presented here produces results for EQE that can be interpreted and explained physically.

4.1.6   HOMO-LUMO wavefunctions

Figure 4.6 represents the spatial distributions of the HOMO-LUMO wavefunctions for the negative phase factor (blue) and positive phase factors (red) for an arrangement of 4 PCBM molecules. The PCBM molecule has a sp_2 hybridization for the carbon since it is a fullerene, and has different combinations of p_z orbitals around the molecule.

The functional group is not involved in the transitions and is perturbing the eigenstates of the fullerene lowering the band gap and pushing down the energy into the visible spectra. Once in the LUMO state, there exists hopping between neighboring molecules acting as a conducting state. The overlaps between HOMO and LUMO states are higher when light is polarized in the **x**-direction.

The HOMO-LUMO wavefunctions show a $\pi - \pi^*$ transition, but the functional group is not involved in this process.
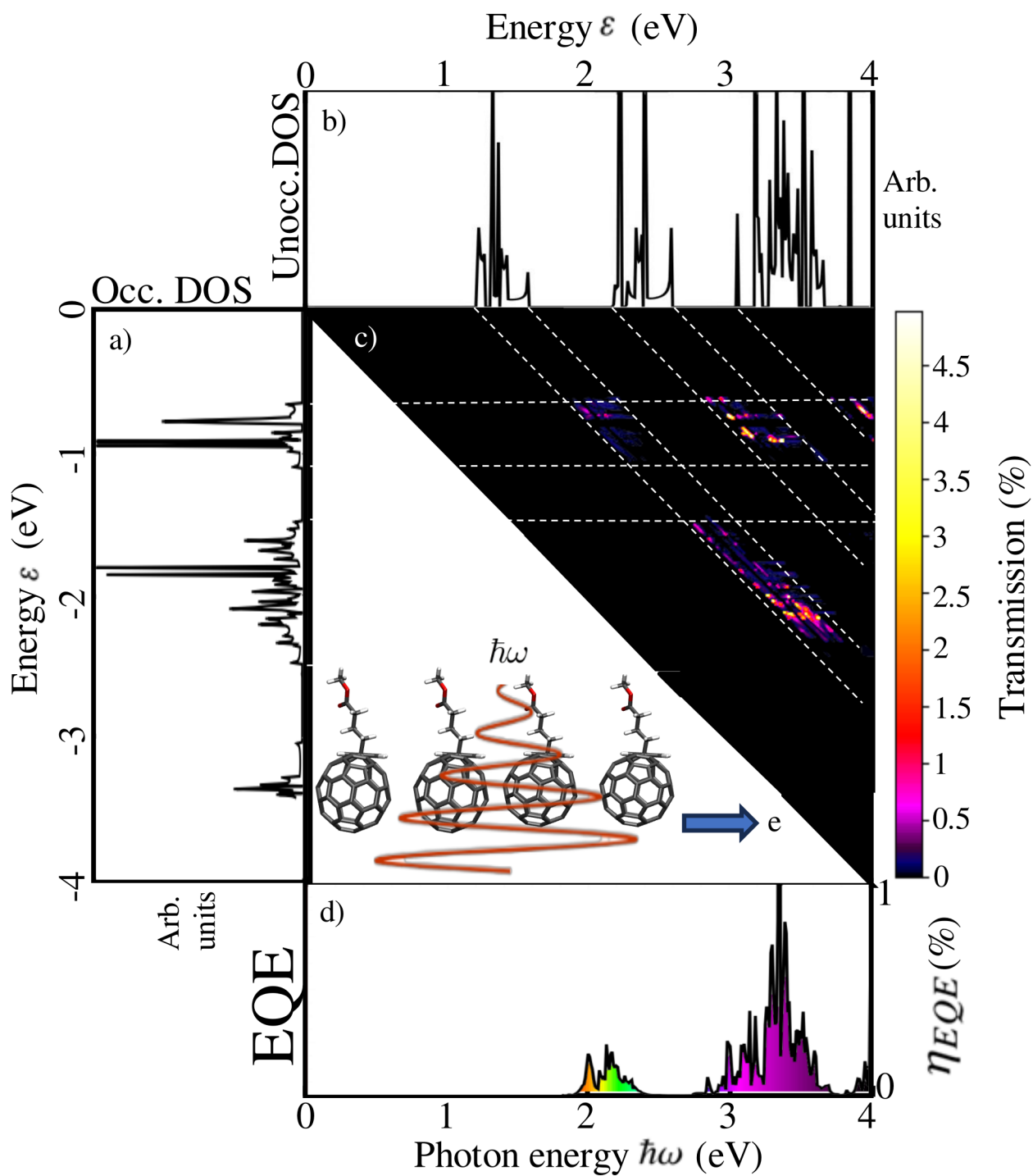
Figure 4.5: a) The occupied DOS in arbitrary units plotted from 0 to 4eV; b) unoccupied DOS in arbitrary units plotted from 0 to -4eV; d) transmission probabilities from 0 to 5%; c) EQE probability with light polarization in the *z*-direction for photon energies from 0 to 4eV.

[H]

LUMO

HOMO

[H]
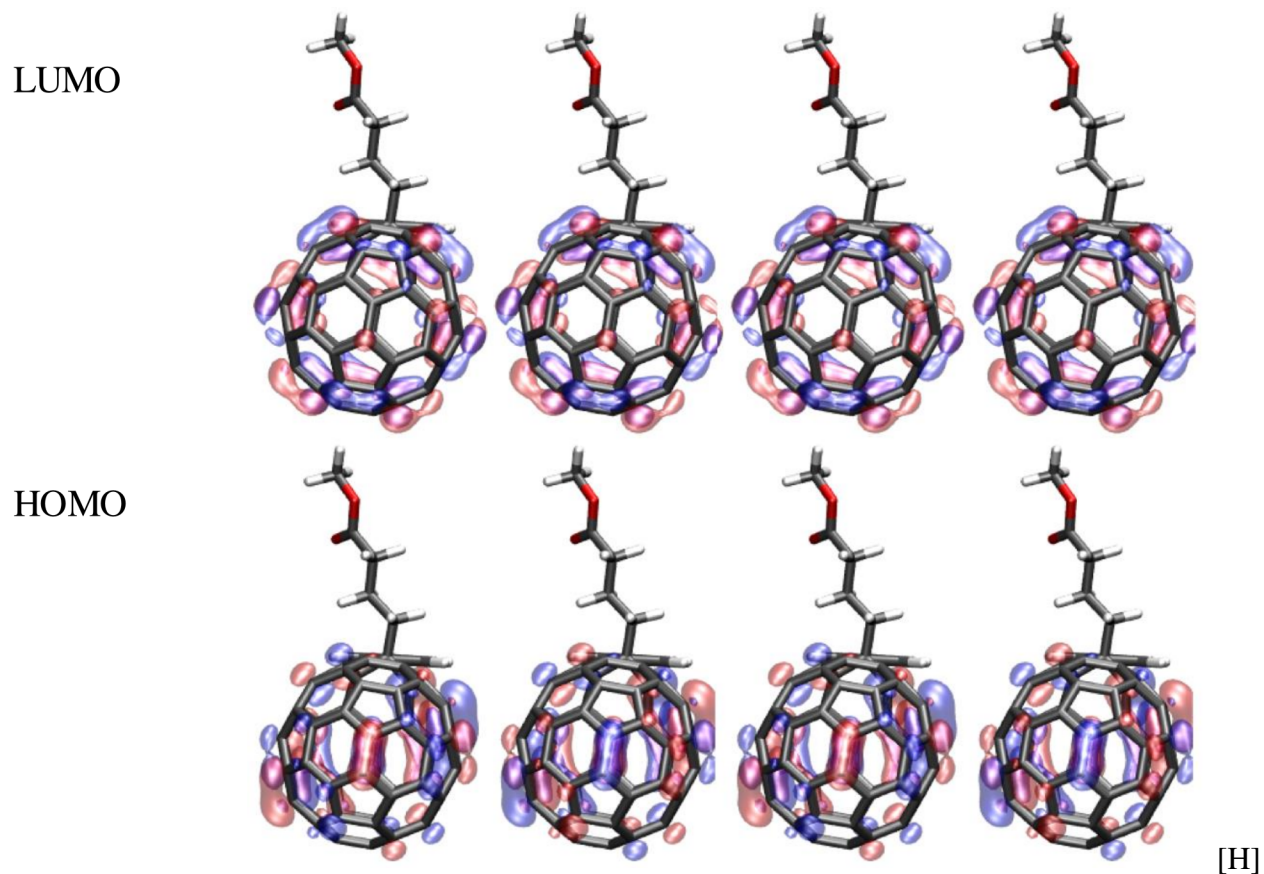
Figure 4.6: Spatial distributions of the wavefunction for the negative and positive phase factors densities of the PCBM molecule HOMO and LUMO. C, O, and H are depicted in grey, red, and white respectively.

Chapter 5

Conclusions

This thesis analyzes an arrangement of an infinite periodic chain of PCBM molecules, its transmission, the occupied and unoccupied density of states, and EQE for light polarized in x, y, and z directions. We have also shown the HOMO and LUMO wavefunction to analyze how the transitions are occurring.

The most stable configuration of a PCBM unit cell was determined by identifying its minimum energy. The minimum energy configuration corresponds to a unit cell size of 9.35 Å. The atomic structure file associated with the most stable unit cell was employed to compute the ground state electronic structure, wavefunctions, Hamiltonian, overlap matrices, and derivative discontinuity correction in the subsequent calculations. This structure was also utilized to obtain a derivative discontinuity correction of 0.57 eV and a band gap of 1.8 eV. Following this, both the derivative discontinuity correction and the associated most stable unit cell were employed to compute EQE calculations, determine the density of occupied and unoccupied states, and assess transmission probabilities. Changing the polarization of the light affects the vector potential $\hat{\mathcal{A}}$ by giving a direction to ∇_r in Eq 4.1.

The EQE plots for light polarization in the x, y, and z directions were also examined. All three plots exhibit similar three energy regions where charge carriers are generated. The first region is observed around 1.8 to 2.4 eV, capturing a small portion of the visible range. The second region spans approximately 2.8 to 3.8 eV, capturing a significant portion of the visible spectrum along with a minor segment of the ultraviolet range, providing the majority of excited electrons. The final EQE structure is situated around 4 eV, corresponding to the ultraviolet region, representing

the smallest contribution to the EQE that can generate charge carriers.

Due to the molecular nature of the system, the excited electrons are expected to stay in the second EQE structure around 2.8 - 3.8 eV. This is because there exists a significant energy difference between the first and second structures that could act as a gap between those low and high-energy charge carriers states. Additionally, it was determined that the EQE plot with the largest intensity is for x polarization, followed by the y direction. Finally, the EQE plot for polarization in z is the one with the lowest intensity.

This can be explained by the relative facility for an electron to do a transition. With the light polarized in the x-direction, an electron can jump more easily from the functional group to the fullerene. For light polarized in the y-direction, the transitions can also occur from the functional group to the fullerene, nevertheless is less efficient compared with polarization in x. Finally, for z-polarization, the electrons excite from the fullerene to the neighboring fullerene, therefore the transmission will be reduced due to the separation distance.

We analyzed the EQE calculation process for 2 PCBM molecules for x, y, and z light polarization and also for a 4 PCBM unit cell with light polarized in z. Plots were categorized: a) occupied DOS versus energy, b) unoccupied DOS versus energy, c) absorption and transmission probability versus energy, d) EQE versus excitation energy. White dashed lines marked energy band boundaries. Three absorption regions were identified: 1.8-2.4 eV from the first LUMO-HOMO overlap, 2.8-3.8 eV from the first LUMO-second HOMO overlap, and 4 eV from the second LUMO-first HOMO overlap. Maximum charge carrier conversion was around 5% for all polarizations.

This model can be applied to test many semiconductor materials used to construct photovoltaic cells. Even if the model does not show the same EQE as in experiments, it gives a trend that can be used for rating the best options for an experimental design. For future work, this model can be implemented together with AI, this way reading large amounts of atomic data sets looking for those materials that give high EQE. This makes it easier to find candidates with better efficiency properties for constructing solar cells. The model can be used as a tool to improve the process of designing better solar cells.

Bibliography

[1] Ministerio de Energía y Minas, ECUADOR CONSOLIDA LA PRODUCCIÓN ELÉCTRICA A PARTIR DE FUENTES RENOVABLES. 2024; `https://www.recursosyenergia.gob.ec/ecuador-consolida-la-produccion-electrica-a-partir-de-fuentes-renovables/#:~:text=Bajo%20este%20precepto%2C%20es%20importante,%2C%20geotermia%2C%20entre%20otras).`

[2] Bube, R. H. *Photovoltaic materials*; World Scientific, 1998; Vol. 1.

[3] Marques Lameirinhas, R. A.; Torres, J. P. N.; de Melo Cunha, J. P. A photovoltaic technology review: history, fundamentals and applications. *Energies* **2022**, *15*, 1823.

[4] Fu, R.; Feldman, D. J.; Margolis, R. M. *US solar photovoltaic system cost benchmark: Q1 2018*; 2018.

[5] Slami, A.; Benramdane, N. *E3S Web of Conferences*; 2021; Vol. 229; p 01005.

[6] Datta, S. *Electronic transport in mesoscopic systems*; Cambridge University Press, 1997.

[7] Coakley, K. M.; McGehee, M. D. Conjugated polymer photovoltaic cells. *Chemistry of materials* **2004**, *16*, 4533–4542.

[8] Li, G.; Shrotriya, V.; Huang, J.; Yao, Y.; Moriarty, T.; Emery, K.; Yang, Y. High-efficiency solution processable polymer photovoltaic cells by self-organization of polymer blends. *Nature materials* **2005**, *4*, 864–868.

[9] Blöchl, P. E. Projector augmented-wave method. *Physical review B* **1994**, *50*, 17953.

[10] Larsen, A. H. *et al.* The atomic simulation environment—a Python library for working with atoms. *Journal of Physics: Condensed Matter* **2017**, *29*, 273002.

[11] Giustino, F. *Materials modelling using density functional theory: properties and predictions*; Oxford University Press, 2014.

[12] Preciado Rivas, M. R. Theoretical optical absorption and electron energy loss spectroscopy using LCAO-TDDFT-K-Ω of chlorophyll and carbon nanotubes. B.Sc. thesis, Yachay Tech University, 2019.

[13] Kratzer, P.; Neugebauer, J. The basics of electronic structure theory for periodic systems. *Frontiers in chemistry* **2019**, *7*, 106.

[14] Kittel, C.; McEuen, P. *Introduction to solid state physics*; John Wiley & Sons, 2018.

[15] Zielinski, T. J.; Harvey, E.; Sweeney, R.; Hanson, D. M. Quantum states of atoms and molecules. 2005.

[16] Combes, J.-M.; Duclos, P.; Seiler, R. The born-oppenheimer approximation. *Rigorous atomic and molecular physics* **1981**, 185–213.

[17] Klippenstein, S. J.; Cavallotti, C. *Computer Aided Chemical Engineering*; Elsevier, 2019; Vol. 45; pp 115–167.

[18] Hohenberg, P.; Kohn, W. Inhomogeneous electron gas. *Physical review* **1964**, *136*, B864.

[19] Woods, N. D.; Payne, M.; Hasnip, P. Computing the self-consistent field in Kohn–Sham density functional theory. *Journal of Physics: Condensed Matter* **2019**, *31*, 453001.

[20] Hartree, D. R. *Mathematical Proceedings of the Cambridge Philosophical Society*; 1928; Vol. 24; pp 111–132.

[21] Glanzmann, L. N. Modelling of polymer-carbon nanotube heterojunctions for photovoltaic applications. Ph.D. thesis, University of the Basque Country UPV/EHU San Sebastián, 2017.

[22] Kohn, W.; Sham, L. J. Self-consistent equations including exchange and correlation effects. *Physical review* **1965**, *140*, A1133.

[23] Fiolhais, C.; Nogueira, F.; Marques, M. A. *A primer in density functional theory*; Springer Science & Business Media, 2003; Vol. 620.

[24] Bagayoko, D. Understanding density functional theory (DFT) and completing it in practice. *AIP Advances* **2014**, *4*.

[25] Dreizler, R. M.; Gross, E. K. *Density functional theory: an approach to the quantum many-body problem*; Springer Science & Business Media, 2012.

[26] Wu, Z.; Cohen, R. E. More accurate generalized gradient approximation for solids. *Physical Review B* **2006**, *73*, 235116.

[27] Perdew, J. P.; Parr, R. G.; Levy, M.; Balduz Jr, J. L. Density-functional theory for fractional particle number: Derivative discontinuities of the energy. *Physical Review Letters* **1982**, *49*, 1691.

[28] Mori-Sánchez, P.; Cohen, A. J. The derivative discontinuity of the exchange-correlation functional. *Physical Chemistry Chemical Physics* **2014**, *16*, 14378–14387.

[29] Perdew, J. P.; Yang, W.; Burke, K.; Yang, Z.; Gross, E. K. U.; Scheffler, M.; Scuseria, G. E.; Henderson, T. M.; Zhang, I. Y.; Ruzsinszky, A.; Zhang, L.; Sun, J.; Csonka, G. I.; Kümmel, S. Understanding band gaps of solids in generalized Kohn–Sham theory. *Proceedings of the National Academy of Sciences* **2017**, *114*, 2801–2806.

[30] Kuisma, M.; Ojanen, J.; Enkovaara, J.; Rantala, T. T. Kohn-Sham potential with discontinuity for band gap materials. *Physical Review B* **2010**, *82*, 115106.

[31] Vanin, M. Projector Augmented Wave Calculations with Localized Atomic Orbitals. Ph.D. thesis, Master thesis, written at CAMD, 2008.

[32] Qin, Q.-H. Green's functions of magneto-electro-elastic plate under thermal loading. *Encyclopedia of Thermal Stresses* **2014**, *38*, 2096–2103.

[33] Arfken, G. B.; Weber, H. J.; Harris, F. E. *Mathematical methods for physicists: a comprehensive guide*; Academic press, 2011.

[34] Weber, H. J.; Arfken, G. B. *Essential mathematical methods for physicists, ISE*; Elsevier, 2003.

[35] Datta, S. The non-equilibrium Green's function (NEGF) formalism: An elementary introduction. 2002.

[36] Datta, S. Nanoscale device modeling: the Green's function method. *Superlattices and microstructures* **2000**, *28*, 253–278.

[37] Paulsson, M. Non equilibrium green's functions for dummies: Introduction to the one particle NEGF equations. *arXiv preprint cond-mat/0210519* **2002**,

[38] Rostgaard, C. The projector augmented-wave method. *arXiv preprint arXiv:0910.1921* **2009**,

[39] Glowacki, I.; Jung, J.; Ulanski, J.; Rybak, A. In *Polymer Science: A Comprehensive Reference*; Matyjaszewski, K., Möller, M., Eds.; Elsevier: Amsterdam, 2012; pp 847–877.

[40] Meir, Y.; Wingreen, N. S. Landauer formula for the current through an interacting electron region. *Physical review letters* **1992**, *68*, 2512.

[41] Mowbray, D.; Morgan, C.; Thygesen, K. S. Influence of O 2 and N 2 on the conductivity of carbon nanotube networks. *Physical review B* **2009**, *79*, 195431.

[42] Enkovaara, J. *et al.* GPAW: a real-space grid implementation of the projector augmented-wave method. *Journal of Physics: Condensed Matter* **2010**, *22*, 253202.

[43] Duncan J. Mowbray,; Jeyson P. Alomoto-Catota,; Daniel E. Gonzalez-Tamayo,; Vito Despoja, External Quantum Efficiency. 2024; `https://gitlab.com/dmowbray/external-quantum-efficiency`, GitLab EQE repository.

[44] Grimme, S.; Antony, J.; Ehrlich, S.; Krieg, H. A consistent and accurate ab initio parametrization of density functional dispersion correction (DFT-D) for the 94 elements H-Pu. *The Journal of Chemical Physics* **2010**, *132*.

[45] Godbout, N.; Salahub, D. R.; Andzelm, J.; Wimmer, E. Optimization of Gaussian-type basis sets for local spin density functional calculations. Part I. Boron through neon, optimization technique and validation. *Canadian Journal of Chemistry* **1992**, *70*, 560–571.

[46] Preciado-Rivas, M. R.; Torres-Sánchez, V. A.; Mowbray, D. J. Optical absorption and energy loss spectroscopy of single-walled carbon nanotubes. *Physical Review B* **2019**, *100*, 235429.

[47] Hüser, F.; Olsen, T.; Thygesen, K. S. Quasiparticle GW calculations for solids, molecules, and two-dimensional materials. *Physical Review B* **2013**, *87*, 235132.